iScience

CellPress
OPEN ACCESS

Article

Smyd3-mediated immuno-modulation in HPV-negative head and neck squamous cell carcinoma mouse models

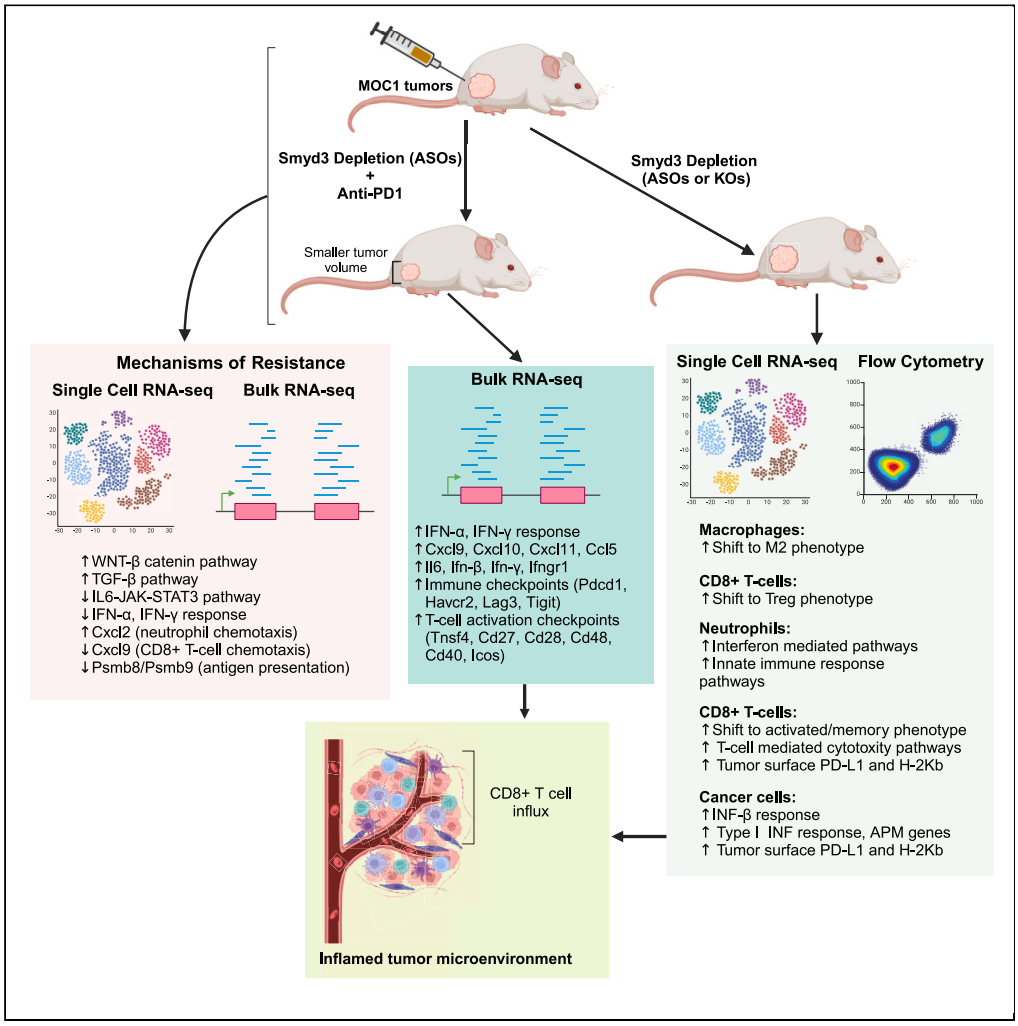

Daniel E. Tsai, Alexei Lovanov, Abdalla Abdelmaksoud, ..., Karim B, Clint T. Allen, Vassiliki Saloura

vassiliki.saloura@nih.gov

Highlights

Smyd3 ASOs reinvigorate CD8$^+$ T-cells and promote anti-tumor neutrophils *in vivo*

Smyd3 ASOs may promote a Treg and M2 macrophage phenotype *in vivo*

Smyd3 ASO and anti-PD-1 combination induces IFN gene signatures in MOC1 tumors

Resistance to Smyd3 ASOs and anti-PD-1 stems from different cell types of the TME

Tsai et al., iScience 27, 110854
September 20, 2024 Published by Elsevier Inc.
https://doi.org/10.1016/j.isci.2024.110854

iScience

CellPress
OPEN ACCESS

Article

Smyd3-mediated immuno-modulation in HPV-negative head and neck squamous cell carcinoma mouse models

Daniel E. Tsai,[1] Alexei Lovanov,[2,3] Abdalla Abdelmaksoud,[2,3] Jawad Akhtar,[1] Mohd Saleem Dar,[1] Marie Luff,[1] Katherine McKinnon,[4] Sohyoung Kim,[5] Yvette Robbins,[6] Angel Huynh,[6] Madhavi Murali,[1] Benjamin Bernard,[1] Andrew Sinkoe,[7] Xiaolin Luo,[8] Karim B,[9] Clint T. Allen,[6] and Vassiliki Saloura[1,10,*]

SUMMARY

SET and MYND-domain containing protein 3 (SMYD3) mediates epigenetic repression of type I IFN response genes in human papillomavirus (HPV)-negative HNSCC cells, and Smyd3 depletion using anti-sense oligonucleotides (ASOs) increases the sensitivity of syngeneic mouse oral carcinoma (MOC1) models to anti-PD-1 therapy. In this study, we utilized single-cell RNA-seq of MOC1 tumors treated with Smyd3 ASOs and found enrichment of type I IFN response pathways in cancer cells, a shift of $CD8^+$ T-cells toward an activated/memory phenotype, and a shift of neutrophils toward an anti-tumorigenic phenotype. Mechanisms of resistance to the Smyd3 ASO and anti-PD-1 combination were derived from cancer cells, macrophages, and $CD8^+$ T-cells, including neutrophil enrichment through the upregulation of *Cxcl2*, repression of *Cxcl9*, and defective antigen presentation. This study sheds light on the immunomodulatory functions of Smyd3 *in vivo* and provides insight into actionable mechanisms of resistance to improve the efficacy of Smyd3 ASOs and anti-PD-1 combination.

INTRODUCTION

Head and neck squamous cell carcinoma (HNSCC) is the sixth most common cancer type in the world, affecting approximately 50,000 patients annually in the United States and having a mortality rate ranked eighth among all cancers.[1] HNSCCs are subdivided into Human papillomavirus (HPV)-negative and HPV-positive tumors. HPV-negative patients have a particularly poor prognosis with an approximately 50% recurrence rate after treatment with standard cisplatin-based chemoradiotherapy and/or surgery.[2] In the recurrent/metastatic setting, pembrolizumab, an immune checkpoint inhibitor that binds to programmed-death-1 (PD-1) and blocks the PD-1/programmed death-ligand 1 (PD-L1) axis, increased the median overall survival from 10.3 months to 13.1 months and was FDA-approved in 2019.[3] However, response rates to pembrolizumab in patients with HPV-negative HNSCC are as low as 19%, underscoring the presence of *de novo* immune escape mechanisms and the urgency to understand and target these mechanisms to increase therapeutic responses to pembrolizumab.

Recent evidence supports the pivotal role of chromatin modifiers in the regulation of antitumor immunity.[4–9] Our group recently reported[10] that loss of SET and MYND-domain containing protein 3 (SMYD3), a protein lysine methyltransferase, increased the sensitivity of HPV-negative-HNSCC cancer cells to interferon-β (IFN-β) and induced transcriptional upregulation of multiple type I IFN response and antigen presentation machinery (APM) genes in human HPV-negative HNSCC cells. Mechanistically, we found that SMYD3 regulates the transcription of Ubiquitin-Like PHD And RING Finger Domain-Containing Protein 1 (UHRF1), a key epigenetic reader of trimethylated lysine 9 on histone H3 (H3K9me3), which binds to H3K9me3-enriched promoters of key immune-related genes, recruits DNMT1 and silences their expression in a DNA-methylation independent manner. SMYD3 further maintains the repression of immune-related genes through the deposition of H4K20me3 within the gene body of these genes. Further, we found that SMYD3 overexpression was associated with decreased tumor $CD8^+$ T cell infiltration and poor response to pembrolizumab in patients with HPV-negative HNSCC. Importantly, the systemic administration of Smyd3 anti-sense oligonucleotides (ASOs), which degrade *Smyd3* mRNA,[11] increased the intratumoral influx of $CD8^+$ T-cells, induced the

[1]Thoracic and GI Malignancies Branch, National Cancer Institute, Bethesda, MD 20892, USA
[2]Collaborative Bioinformatics Resource (CCBR), Center for Cancer Research (CCR), National Cancer Institute (NCI), National Institutes of Health, Bethesda, MD 20892, USA
[3]Advanced Biomedical Computational Science, Frederick National Laboratory for Cancer Research, Frederick, MD 20892, USA
[4]Center for Cancer Research Vaccine Branch Flow Cytometry Core, National Cancer Institute, Bethesda, MD 20892, USA
[5]Laboratory of Receptor Biology and Gene Expression, National Cancer Institute, Bethesda, MD 20852, USA
[6]Head and Neck Section, Surgical Oncology Program, Center for Cancer Research, National Cancer Institute, National Institutes of Health, Bethesda, MD 20852, USA
[7]Center for Immuno-Oncology, National Cancer Institute, National Institutes of Health, Bethesda, MD 20852, USA
[8]Ionis Pharmaceuticals, Inc., Carlsbad, CA 92010, USA
[9]Molecular Histopathology Laboratory, National Institutes of Health, Frederick, MD 21702, USA
[10]Lead contact
*Correspondence: vassiliki.saloura@nih.gov
https://doi.org/10.1016/j.isci.2024.110854

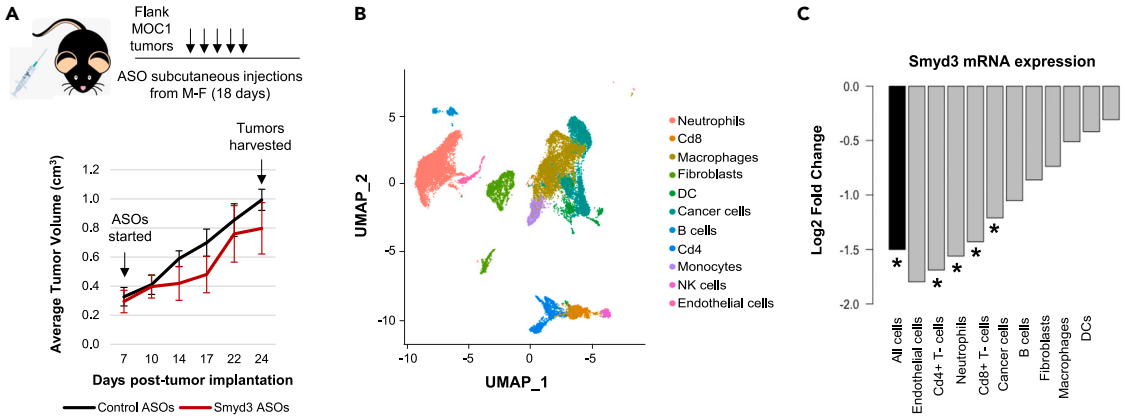

Figure 1. Single cell RNA-sequencing of MOC1 tumors treated with Smyd3 ASOs reveals distinct cancer and immune cell types and differential efficacy of Smyd3 ASOs based on cell type

(A) Design of mouse experiment. Flank MOC1 tumors were established in C57BL/6 mice, and control or Smyd3 ASO treatment was started with subcutaneous injections. 3 tumors were treated per condition. Mice were sacrificed and tumors harvested 24 days post-implantation (18 days of treatment).

(B) UMAP embedding showing 24,400 single cells obtained from MOC1 tumors treated with control (n = 3) or Smyd3 ASOs (n = 3) for 18 days. Cell types were identified using clustering and marker gene expression analysis.

(C) Log2 fold change of *Smyd3* mRNA levels in individual cell types of MOC1 tumors treated with Smyd3 or control ASOs. *$p < 0.05$, adjusted p-value.

upregulation of the protein levels of PD-1 on $CD8^+$ T-cells, and PD-L1 and H2-Kb on MOC1 cells, and sensitized MOC1 flank tumors to anti-PD-1 therapy in a syngeneic mouse model, which recapitulates human anti-PD-1 resistant HPV-negative HNSCC.[12]

Despite a growing understanding of the role of SMYD3 as an oncogenic driver in multiple cancer types[5,13–20] its role in antitumor immunity is understudied. Smyd3 ASOs represent a promising drug platform that could enable the translation of SMYD3 depletion in a patient setting.[11,20] While pembrolizumab is the first-line standard of care treatment for patients with HPV-negative HNSCC, response rates are low, thus translational efforts are necessary to improve therapeutic efficacy. Our previous study[10] showed that Smyd3 ASOs sensitized the anti-PD-1 resistant syngeneic flank MOC1 mouse tumor model to anti-PD-1 therapy. In this study, we aimed to systematically interrogate the effects of ASO- or CRISPR knockout-induced Smyd3 depletion within cancer and immune cell populations of the tumor microenvironment (TME) at the single-cell level in this mouse tumor model. We also evaluate the global changes in the TME of MOC1 tumors treated with Smyd3 ASOs and anti-PD-1 and elucidate potential mechanisms of resistance of MOC1 tumors to the combination treatment. We shed light on how each cell type within the TME may contribute to resistance through different mechanisms, and provide insights into combinatorial approaches that could increase the therapeutic efficacy of the Smyd3 ASO and anti-PD-1 combination treatment in patients with HPV-negative HNSCC.

RESULTS

Smyd3 ASOs demonstrate differential efficacy in depleting *Smyd3* mRNA based on cell type in MOC1 tumors

We previously showed that, although the treatment of flank MOC1 tumors with the systemic administration of control or Smyd3 ASO monotherapy induced intratumoral influx of $CD8^+$ T-cells and upregulation of tumor cell PD-L1 and MHC class I protein levels, it did not induce significant shrinkage in the MOC1 tumor volumes.[10] However, the combination treatment of Smyd3 ASOs with anti-PD-1 rendered significant tumor shrinkage compared to treatment with control ASOs and anti-PD-1. To evaluate the differential effects of Smyd3 ASOs on individual cell types within MOC1 tumors and identify potential mechanisms through which Smyd3 ASOs sensitize these to anti-PD-1 therapy, a mouse experiment was conducted with 3 MOC1 tumors treated with control ASOs and 3 MOC1 tumors treated with Smyd3 ASO monotherapy. Mice were sacrificed 24 days post-implantation (18 days of ASO treatment), tumors were resected, and single-cell RNA sequencing of all tumors was conducted (Figures 1A and S1). 11 different cell types were discernible in the UMAP analysis of all MOC1 tumors (Figures 1B and S2A). As expected, *Smyd3* mRNA levels were significantly decreased by 65% in MOC1 tumors treated with Smyd3 ASOs compared to control (Figures 1C and Table S1), confirming that the Smyd3 ASOs induced a pharmacodynamically adequate effect within MOC1 tumors.

We then evaluated the effect of Smyd3 ASOs on the *Smyd3* mRNA levels of individual cell types within MOC1 tumors. $CD8^+$ T-cells, $CD4^+$ T-cells, neutrophils, and cancer cells demonstrated at least a 50% decrease in *Smyd3* mRNA expression levels (Figure 1C and Table S1). Macrophages demonstrated an approximately 40% decrease in *Smyd3* mRNA levels with a trend for statistical significance (adjusted p-value = 0.09). Interestingly, dendritic cells (DCs), monocytes, and NK cells did not demonstrate a significant decrease in *Smyd3* mRNA expression levels, possibly suggesting decreased uptake of the Smyd3 ASOs by these cell types. *Smyd3* mRNA levels were similarly decreased by 72% in endothelial cells, but this value did not reach statistical significance. These findings support that Smyd3 ASOs may have variable uptake by cell type, with cancer cells, $CD8^+$ and $CD4^+$ T-cells, and neutrophils demonstrating the most efficient uptake and thus resulting in a "deeper" depletion of *Smyd3* mRNA levels.

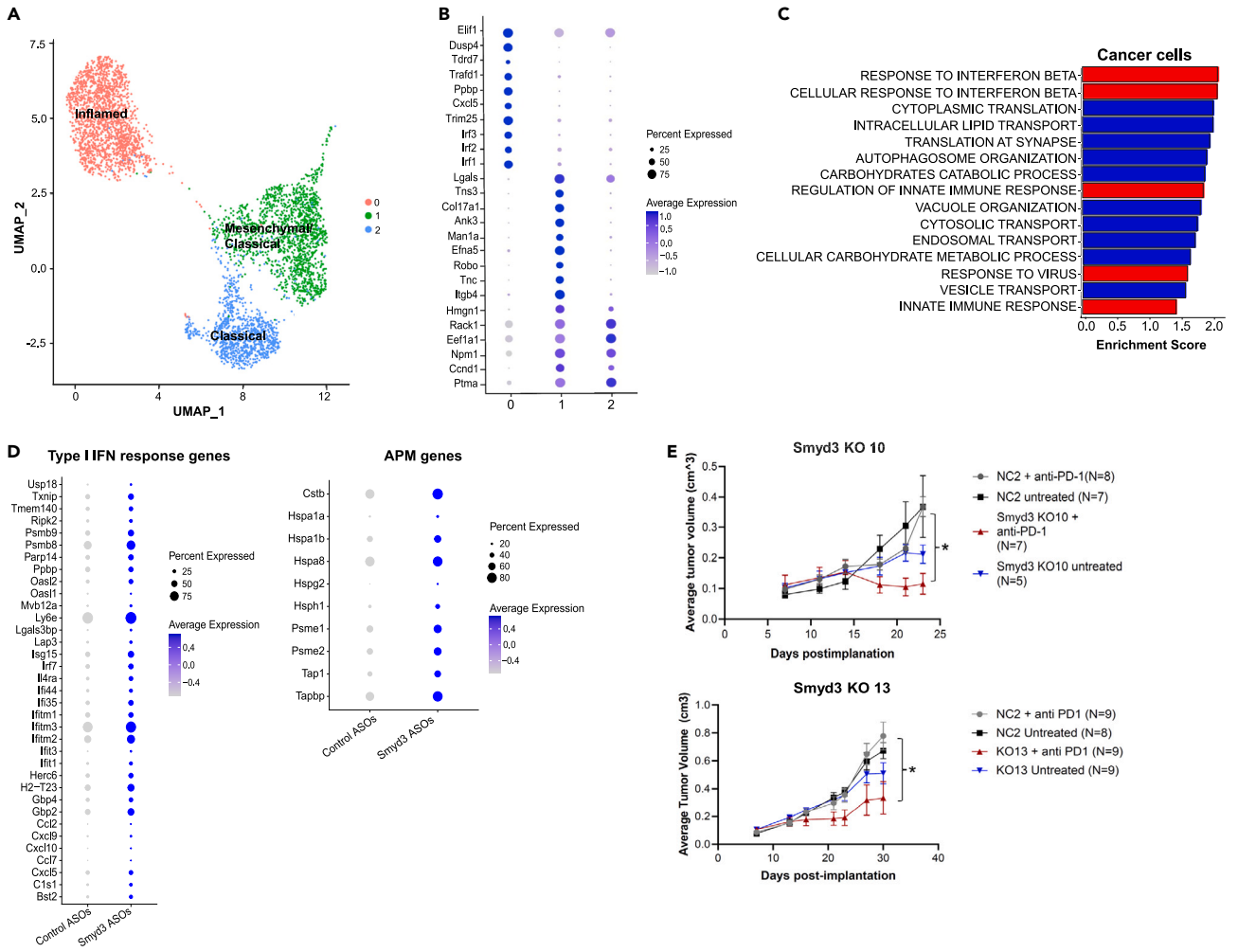

Figure 2. Smyd3 ASO treatment of cancer cells in MOC1 tumors induces the enrichment of type I IFN response pathways and sensitizes MOC1 tumors to anti-PD-1 therapy

(A) UMAP of cancer cells. Single-cell RNA sequencing was conducted in control (n = 3) and Smyd3 (n = 3) ASO treated MOC1 tumors. Three distinct transcriptomic clusters were identified: inflamed, mesenchymal/classical, and classical cluster.

(B) Dotplot of selected gene markers characterizing each cancer cell cluster.

(C) GSEA of all cancer cells of MOC1 tumors treated with Smyd3 versus control ASOs. Enrichment scores (ES) of Gene Ontology Biological Processes (GOBP) gene sets are shown. Red bars indicate positive enrichment; blue bars indicate negative enrichment.

(D) Dotplots showing expression of type I IFN response and antigen presentation machinery (APM) genes in cancer cells of MOC1 tumors treated with control or Smyd3 ASOs.

(E) Average tumor volume growth curves of NC2 and KO10 (left curve) or NC2 and K013 tumors (right curve) treated with anti-PD-1. C57BL/6 mice were injected with NC2 and KO10 or NC2 and KO13 cells in the right flank, and, once they reached an average tumor volume of 0.01cm3, treatment with anti-PD-1 was started. Number of mice per group is shown in parentheses (N). Data are represented as mean ± SEM. NC2/KO10: unpaired t-test, $^{**}p$ = 0.002, NC2/KO13: unpaired t-test, $^{*}p$ = 0.01.

Smyd3 ASO treatment of MOC1 tumors induces the upregulation of immune-related gene expression in MOC1 cancer cells

We then evaluated the effect of Smyd3 ASOs on the cancer cell compartment of MOC1 tumors treated with Smyd3 ASO compared to control ASO monotherapy. UMAP analysis of MOC1 cancer cells identified three distinct clusters (0, 1, and 2) (Figures 2A, 2B, and S2B; Tables S2 and S3). Gene Set Enrichment Analysis (GSEA) revealed that cluster 0 was enriched in immune-related pathways, such as Interferon alpha response, Interferon gamma response and TNFa signaling via NFKB Hallmark pathways (Figure S3A), reminiscent of the inflamed expression subtype previously reported using bulk RNA-seq analysis of HPV-negative HNSCC human tumor samples.[21,22] Accordingly, the relative up-regulation of certain immune-related genes, such as *Cxcl5* which codes for a potent chemoattractor of $CD8^+$ T-cells, *Ppbp*, which codes for pro-platelet basic protein which potently attracts and activates neutrophils, and type I IFN-response genes *Irf1*, *Irf2*, *Irf7* and *Trim 25*, was observed compared to clusters 1 and 2 (Figures 2B and Table S3). Cluster 1 was characterized by the enrichment of EMT-related pathways,

such as the Wnt/β catenin signaling and the Epithelial-mesenchymal transition Hallmark pathways (Figure S3), with the upregulation of multiple EMT-related genes, such as *Itgb4*, *Tnc*, *Robo2*, *Man1a*, *Ank3* and *Col17a1* (Figure 2B and Table S3), supporting a mesenchymal phenotype. Enrichment of cell cycle related pathways, such as the E2F targets, G2M checkpoint and MYC targets Hallmark pathways (Figure S3B), with the upregulation of cell-cycle related genes, such as *Ccnd1*, *Npm1*, and *Eef1a1* (Figures 2B and Table S3), was also observed, suggestive of concurrent features of the classical expression subtype. Finally, cluster 2 demonstrated enrichment in cell-cycle-related pathways (G2M-checkpoint Hallmark pathways) with the upregulation of cell-cycle related genes (Figures S3C, 2B, and Table S3), supporting a classical phenotype. These findings suggest that cancer cells within MOC1 tumors have expression features representative of the inflamed, mesenchymal, and classical subtypes.

Comparison of cell abundance for each cancer cell cluster between control- and Smyd3 ASO- treated MOC1 tumors showed no significant differences between the two treatment conditions, supporting that treatment with Smyd3 ASOs did not affect the cancer cell phenotypes within the TME of MOC1 tumors (Figure S4 and Table S2). However, in accordance to our previously published study,[10] cancer cells treated with Smyd3 ASOs compared to control ASOs demonstrated the positive enrichment of immune-related pathways, such as the Interferon mediated signaling and the Innate immune response pathways (Gene Ontology Biological Processes) (Figure 2C), with the upregulation of multiple type I IFN response and APM genes (Figure 2D and Tables S3 and S4). These results suggest that, while *in vivo* Smyd3 ASO treatment does not decrease tumor growth, it may enhance immunogenicity by increasing the expression of type I IFN response and APM genes in MOC1 cancer cells.

Smyd3 knockout in the cancer cell compartment of MOC1 mouse tumors enhances the antitumor efficacy of anti-PD-1 treatment

To evaluate whether Smyd3 depletion within the cancer cell compartment of MOC1 tumors suffices to induce the antitumor effects observed with the Smyd3 ASO + anti-PD-1 combination therapy *in vivo*, we generated Smyd3 knockout (KO) MOC1 cell lines using CRISPR. Two *Smyd3* KO clones (KO10 and KO13) were utilized in two independent *in vivo* mouse experiments, comparing the growth of control (NC2) tumors and the KO10 or KO13 tumors treated with anti-PD-1 therapy. The growth of *Smyd3* KO MOC1 tumors treated with anti-PD-1 (KO10 + anti-PD-1, KO13 + anti-PD-1 groups) was significantly decreased compared to control tumors treated with anti-PD-1 (NC2 + anti-PD-1) (Student's t test; NC2/KO10 + anti-PD-1, $p = 0.011$; NC2/KO13 + anti-PD-1, $p = 0.002$) (Figure 2E). These results suggest that Smyd3 depletion in cancer cells alone is enough to significantly increase the anti-tumor efficacy of anti-PD-1 treatment in MOC1 tumors.

Interestingly, similar to what we previously reported with Smyd3 ASO monotherapy,[10] *Smyd3* KO alone induced a decrease in the average MOC1 tumor volume, however, this was not statistically significant (day 25, KO10 MOC1 average tumor volume = 0.212cm^3 compared to NC2 MOC1 average tumor volume = 0.368cm^3, Student's t test, $p = 0.19$; day 30, KO13 MOC1 average tumor volume = 0.512cm^3 compared to NC2 MOC1 average tumor volume = 0.673cm^3, Student's t test, $p = 0.12$) (Figure 2E).

Smyd3 knockout within the cancer cell compartment increases the influx of CD8$^+$ T-cells and upregulates the expression of Pd-l1 and H-2Kb in MOC1 tumors

To assess the effects of *Smyd3* KO of the cancer cell compartment in the tumor microenvironment of MOC1 tumors, multicolor flow cytometry was conducted on tumors that were generated using the control NC2 and *Smyd3* KO13 cell lines treated with anti-PD-1 (NC2 + anti-PD-1, KO13 + anti-PD-1) or not (NC2, KO13) as described above (Figure 2E). Flow cytometry revealed significant upregulation of MHC class I H-2Kb in *Smyd3* KO MOC1 tumor cells compared to control cells (NC2) both in the presence (unpaired t-test, $p = 0.001$) or absence (unpaired t-test, $p = 0.0002$) of anti-PD-1, supporting increased antigen presentation capacity of the *Smyd3* KO cancer cells regardless of anti-PD-1 therapy (Figure 3A). Additionally, the percentage of PD-L1 expressing *Smyd3* KO cancer cells was significantly increased compared to control cells, particularly in the presence of anti-PD-1 (unpaired t-test, $p < 0.0001$), suggesting an increase in the interferon responsiveness of the cancer cells (Figure 3A). CD8$^+$ and CD4$^+$ T cell influx was also significantly increased in the *Smyd3* KO MOC1 tumors, with a more pronounced increase in the presence of anti-PD-1 (CD8$^+$ T-cells, unpaired t-test, $p = 0.007$; CD4$^+$ T-cells, unpaired t-test, $p = 0.005$) (Figures 3B–3D). A trend for the upregulation of PD-1 on CD8$^+$ T-cells was also observed (unpaired t-test, $p = 0.05$) (Figure 3C). Interestingly, a decrease in the infiltration by granulocytic myeloid derived suppressor cells (gMDSCs) was observed both in the presence (unpaired t-test, $p = 0.06$) or absence (unpaired t-test, $p = 0.0035$) of anti-PD-1 (Figure 3E).

To evaluate whether CD8$^+$ and/or CD4$^+$ T-cells are necessary for the antitumor effect observed with the anti-PD-1 treatment of the *Smyd3* KO MOC1 tumors, a CD8$^+$ and CD4$^+$ T cell depletion experiment was conducted. Specifically, KO10 MOC1 cells were implanted in the flanks of C57BL/6 mice and once tumors reached an average tumor volume of 0.1cm^3, treatment was initiated with either anti-PD-1, anti-PD-1 and anti-CD8, or anti-PD-1 and anti-CD4. Importantly, CD8$^+$ but not CD4+T cell depletion completely abrogated the anti-tumor efficacy of anti-PD-1 treatment on *Smyd3* KO MOC1 tumors (Figure 3F). This finding strongly supports that CD8$^+$ T-cells, but not CD4$^+$ T-cells, are necessary for the anti-tumor efficacy of Smyd3 depletion.

Smyd3 ASO treatment of MOC1 tumors induces the upregulation of pathways associated with cytotoxicity in CD8$^+$ T-cells

To evaluate the effects of Smyd3 ASO treatment of MOC1 tumors in the T cell compartment, UMAP analysis focused on T-cells was conducted and cells were subclustered into 10 distinct clusters: progenitor CD8$^+$ T-cells (cluster 1), exhausted CD8$^+$ T-cells (cluster 2, exh1 and cluster 6, exh2), regulatory T-cells (Tregs) (cluster 0), progenitor CD4$^+$ T-cells (cluster 3), type 1 T-helper (Th1)s CD4$^+$ T-cells (cluster 5), NK cells (cluster 4), progenitor/central memory (cluster 7), effector memory (cluster 8) and naive T-cells (cluster 9) (Figures 4A and 4B).

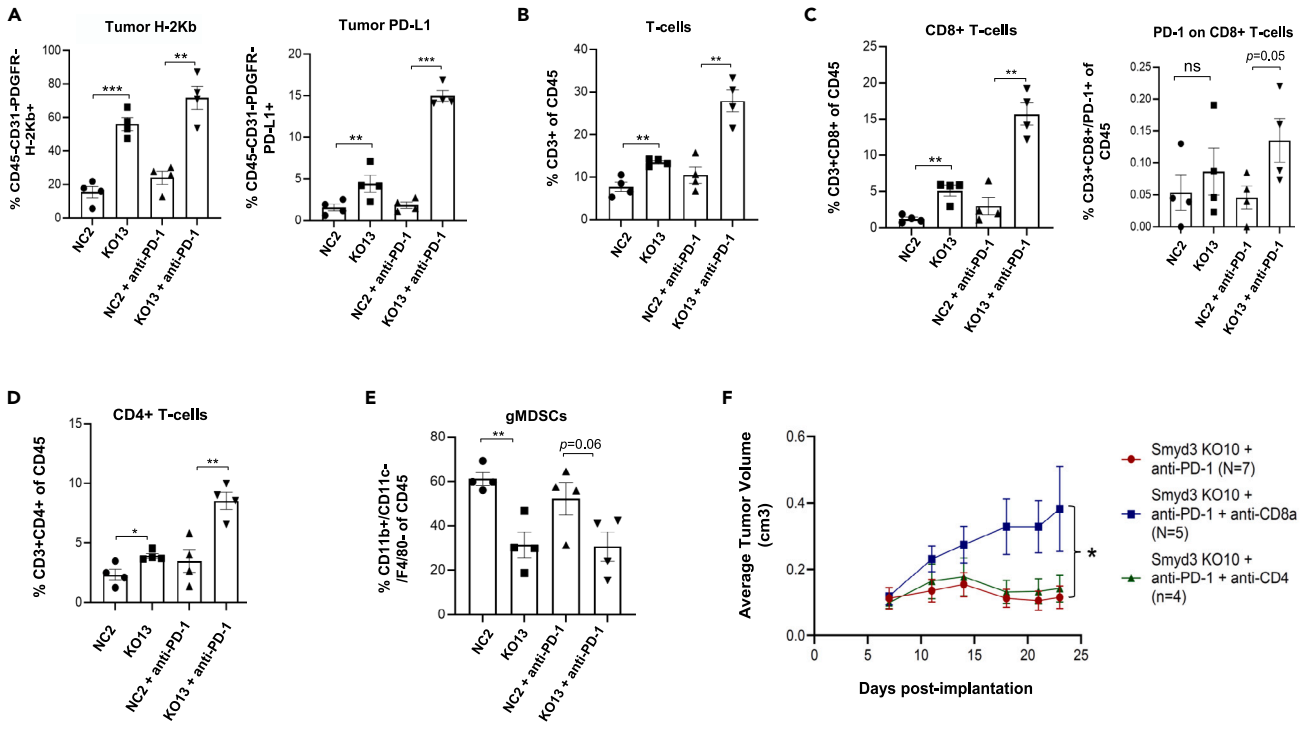

Figure 3. *Smyd3* KO in the cancer cell compartment of MOC1 tumors induces an influx of CD8$^+$ T-cells which are necessary for the anti-tumor efficacy of anti-PD-1 therapy

(A–E) Multicolor flow cytometry of control (NC2) and *Smyd3* KO (KO13) MOC1 tumors treated or not with anti-PD-1. C57BL/6 mice were injected with NC2 and KO13 cells in the right flank, and, once they reached an average tumor volume of 0.01cm3, treatment with anti-PD-1 was started. 34 days after tumor implantation, mice were sacrificed, and tumors were surgically resected and processed into single-cell suspensions. Cell suspensions were stained with antibodies and multicolor flow cytometry was conducted (day 34 post-tumor implantation, $n = 4$ per group). Data are represented as mean ± SEM. NC2: control, KO13: *Smyd3* KO. (A) % of CD45$^-$CD31-PDGFR-H-2Kb+ or PD-L1+ MOC1 cells, (B) % of CD3$^+$ CD45$^+$ cells, (C) % of CD3$^+$CD8$^+$ and CD3$^+$CD8+/PD-1+ of CD45$^+$ cells, (D) % CD3$^+$CD4$^+$ of CD45$^+$ cells, (E) % of CD11b+/CD11c-/F4/80- of CD45$^+$ cells. Unpaired t-tests between NC2 and KO13 or NC2 + anti-PD-1 and KO13 + anti-PD-1 conditions: *$p < 0.05$, **$p < 0.01$, ***$p < 0.001$.

(F) CD8$^+$ T cell depletion abrogates the anti-tumor efficacy of anti-PD-1 in *Smyd3* KO MOC1 tumors. C57BL/6 mice were injected with NC2 and KO10 cells in the right flank, and, once they reached an average tumor volume of 0.01cm3, mice were randomized into three groups, and treatment with anti-PD-1, anti-PD-1, and anti-CD8 or anti-PD-1 and anti-CD4 was started. Unpaired t-test, *$p = 0.039$.

To dissect the effect of Smyd3 ASOs on these T cell clusters, we assessed changes in the cell abundance of each T cell cluster as well as gene expression changes induced by Smyd3 ASO treatment at the cluster level. No significant differences were observed in the cell abundance of each of the CD8$^+$ T cell clusters (progenitor, exhausted, and central memory) after Smyd3 ASO treatment (Figure S2C, S4B; Table S2). However, GSEA including all CD8$^+$ T cell clusters revealed enrichment of pathways related to T cell mediated cytotoxicity after Smyd3 ASO treatment (Figure 4C). Further analysis focused on cluster gene markers as well as selected immune-related gene expression changes demonstrated that Smyd3 ASO treatment induced the upregulation of *Gzmb* with the concurrent upregulation of *Pdcd1* in exhausted CD8$^+$ T-cells (cluster 2), indicating activation and increased cytotoxic activity of this cluster (Figure 4D and Table S5). Upregulation of *Il7r*, which promotes survival, was also observed, suggesting that Smyd3 ASO treatment may also increase the survival capacity of exhausted CD8$^+$ T-cells. *Ccnd3* expression levels were upregulated, signifying increased the proliferation of cluster 2 CD8$^+$ T-cells. T-cells with a progenitor/central memory phenotype (cluster 7), characterized by a higher expression of *Tcf7*, *Ccr7*, and *Il7r*, demonstrated the upregulation of *Ifgr1* and *Il2rb* upon Smyd3 ASO treatment, suggesting a shift toward an activated/memory phenotype (Figure 4D and Table S5). In the progenitor CD8$^+$ T-cells (cluster 1), Smyd3 ASO treatment induced the upregulation of *Ccnd3*, suggesting increased the proliferation of this cluster (Table S5). These findings were further corroborated by dedicated GSEA analysis focusing on cluster 2 and cluster 7 of CD8$^+$ T-cells, showing the enrichment of Ifn-a and Ifn-g response pathways (Hallmark gene sets) (Figure S5).

Regarding the effect of Smyd3 ASOs on CD4$^+$ T-cells, similarly, Smyd3 ASOs did not affect the cell abundance of Th1, Tregs, or progenitor CD4$^+$ T-cells (Figure S4B; Table S2). Interestingly, GSEA of all CD4$^+$ T-cells showed the enrichment of tolerance induction pathways, indicating a shift toward Treg differentiation (Figure 4E). Further interrogation of expression changes of Th1 and Treg defining genes in cluster 5 revealed that Smyd3 ASO treatment induced the expression of *Ctla4*, suggesting a shift of differentiation away from a Th1 phenotype and toward a Treg phenotype. Cell cycle-related genes *Eea1* and *Ccnd3*, as well as the anti-apoptotic gene *Bcl2*, were also upregulated, suggesting

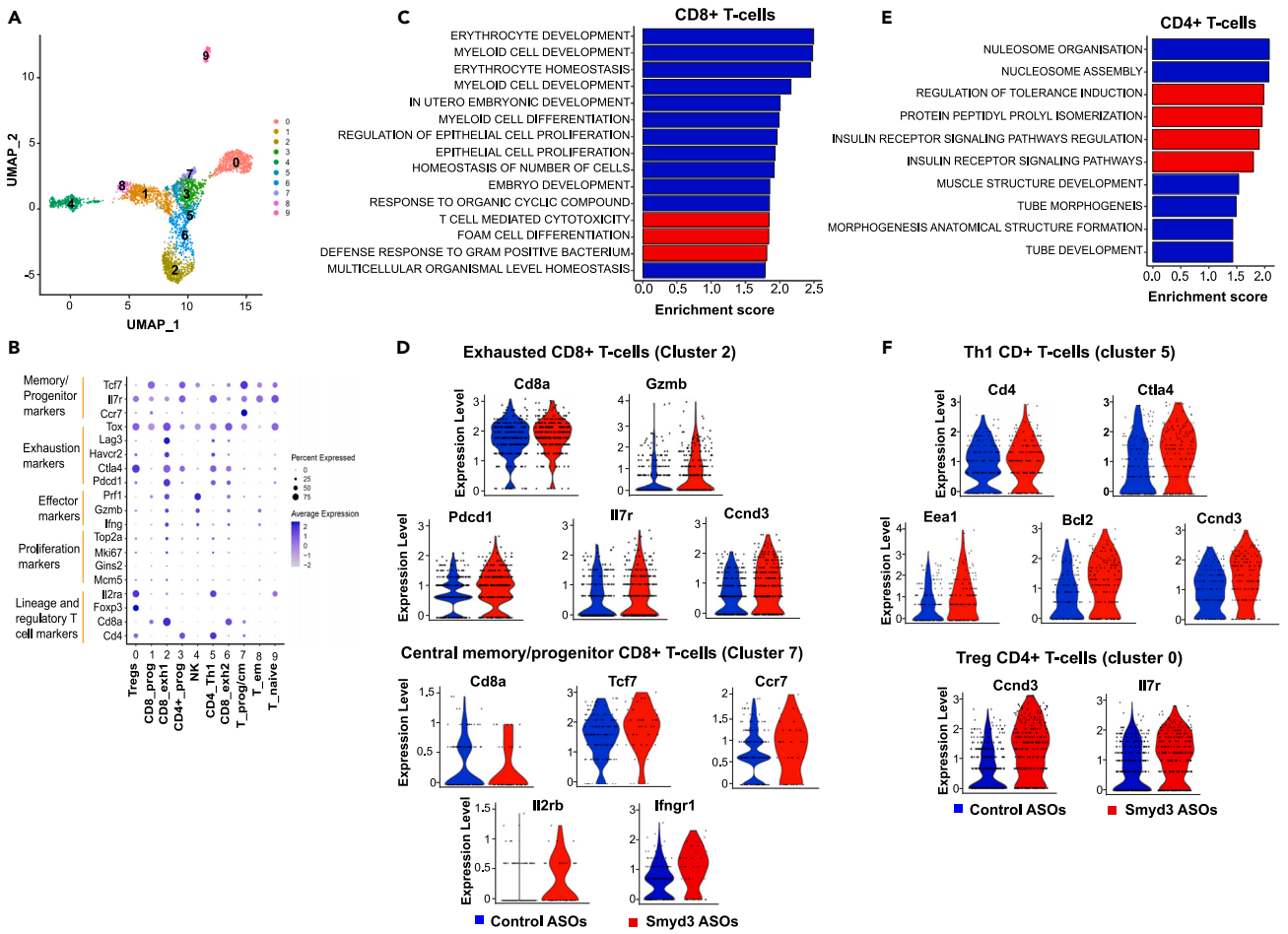

Figure 4. Smyd3 ASO treatment of CD8$^+$ T-cells in MOC1 tumors induces a shift toward an activated/memory phenotype

(A) UMAP embedding of T-cells colored by cluster identity in MOC1 tumors treated with control or Smyd3 ASOs (n = 3 per condition).

(B) Dot plot showing relative expression of selected T cell genes across identified T cell clusters. Circle color corresponds to scaled average expression; circle size denotes the fraction of cells with non-zero gene expression of the corresponding gene.

(C) GSEA of all CD8$^+$ T-cells of MOC1 tumors treated with Smyd3 versus control ASOs. Enrichment scores (ES) of GOBP gene sets are shown. Red bars indicate positive enrichment; blue bars indicate negative enrichment.

(D) Violin plots of selected genes expressed in cluster (2) of exhausted CD8$^+$ T-cells and in cluster 7 of central memory/progenitor CD8$^+$ T-cells.

(E) GSEA analysis of all CD4$^+$ T-cells in MOC1 tumors treated with Smyd3 versus control ASOs. Enrichment scores (ES) of GOBP gene sets are shown. Red bars indicate positive enrichment; blue bars indicate negative enrichment.

(F) Violin plots of selected genes expressed in cluster (5) of Th1 CD4$^+$ T-cells and in cluster 0 of Treg CD4$^+$ T-cells.

a higher proliferative potential of this cluster (Figure 4F and Table S5). Consistently, Tregs (cluster 0) showed the upregulation of *Ccnd3* and *Il7r*, indicating increased proliferative and survival potential with Smyd3 ASO treatment (Figure 4F and Table S5).

Smyd3 ASO treatment of MOC1 tumors may enhance an anti-tumor neutrophil phenotype

Three clusters of neutrophils were identified (UMAP subtypes 0–2) (Figures 5A and 5B). Cluster 0 displayed a gene expression module more consistent with the anti-tumor (N1) phenotype, whereas cluster 1 had a gene expression module consistent with the pro-tumor (N2) phenotype.[23–25] Cluster 2 was more undifferentiated. While no significant difference was observed in the percentages of each neutrophil cluster (Figure S4C and Table S2), GSEA including all clusters treated with Smyd3 versus control ASOs showed enrichment in pathways related to the regulation of IFN-mediated signaling, innate immune response, cell adhesion, cell adhesion, and lymphocyte activation (Figure 5C). Consistently, differential gene expression analysis focusing on the more undifferentiated cluster 2 neutrophils comparing Smyd3 versus control ASO treated cells showed the downregulation of *Arg2* and *Ccl3*, markers of N2 differentiation (Figure 5D and Table S5).[25] While these data suggest that Smyd3 ASOs may shift neutrophil differentiation toward an anti-tumor phenotype, pathways related to metabolites and energy precursors were negatively enriched (Figure 5C). Accordingly, glycolytic pathway enzymes, such as hexokinase-2 and aldolase a, were downregulated, implying decreased metabolic activity of neutrophils (Table S5).

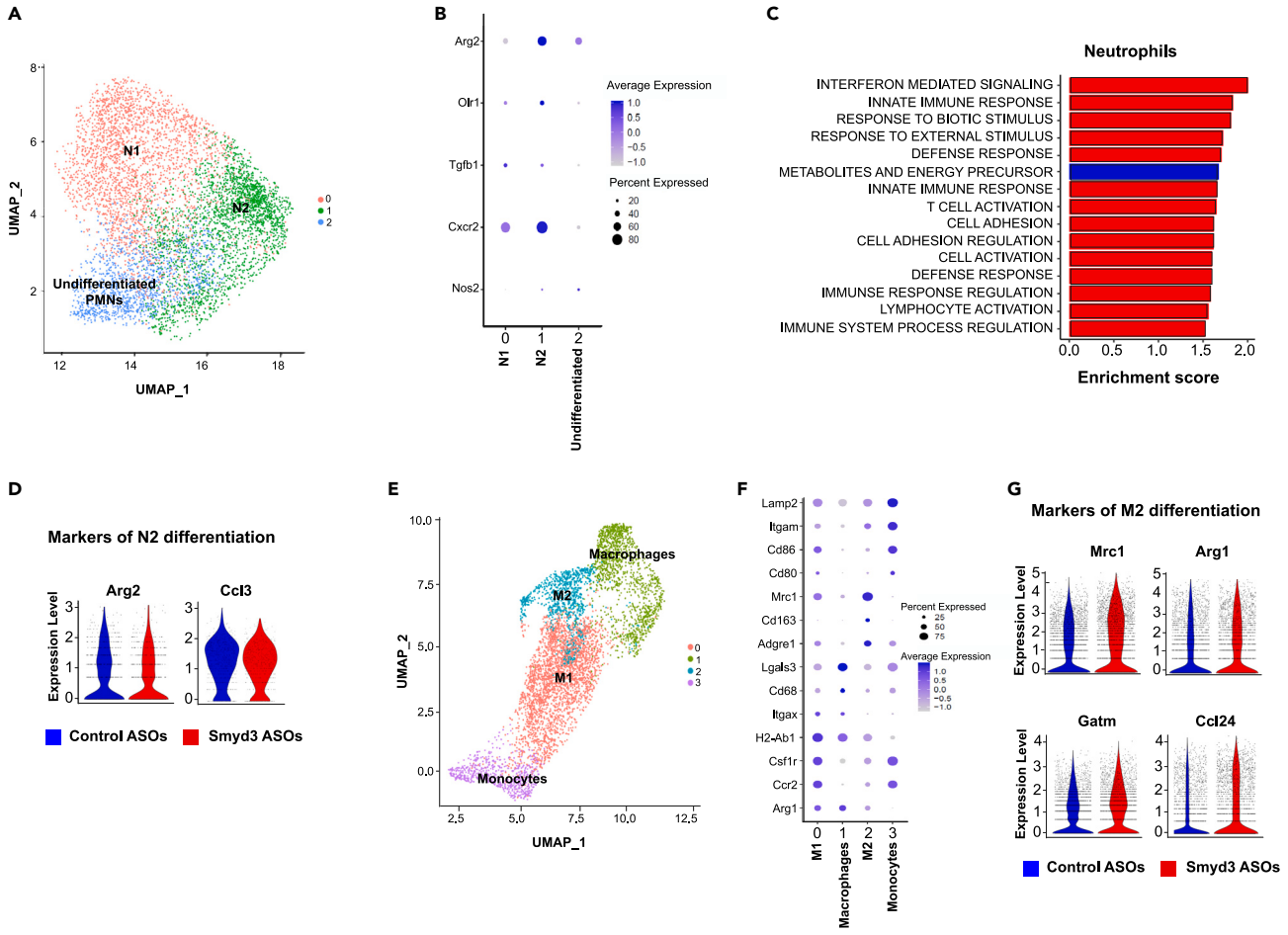

Figure 5. Smyd3 ASOs enhance neutrophil activation pathways but may promote an M2 macrophage phenotype in MOC1 tumors

(A) UMAP embedding of neutrophils colored by cluster identity in MOC1 tumors treated with control or Smyd3 ASOs (n = 3 per condition).

(B) Dot plot showing relative expression of selected genes across identified neutrophil clusters. Circle color corresponds to scaled average expression; circle size denotes the fraction of cells with non-zero gene expression of the corresponding gene.

(C) GSEA of all neutrophil clusters of MOC1 tumors treated with Smyd3 versus control ASOs. Enrichment scores (ES) of GOBP gene sets are shown. Red bars indicate positive enrichment; blue bars indicate negative enrichment.

(D) Violin plots of selected genes associated with N2 neutrophil differentiation expressed in all neutrophil clusters.

(E) GSEA of all mononuclear myeloid cells of MOC1 tumors treated with Smyd3 versus control ASOs. Enrichment scores (ES) of GOBP gene sets are shown. Red bars indicate positive enrichment; blue bars indicate negative enrichment.

(F) Dotplot showing relative expression of selected genes across identified mononuclear myeloid clusters.

(G) Violin plots of selected genes expressed associated with M2 neutrophil differentiation expressed in all mononuclear myeloid clusters.

Smyd3 ASO treatment of MOC1 tumors may induce an M2 macrophage phenotype

Four clusters of mononuclear myeloid cells were visualized using UMAP analysis: M1 cells (cluster 0), M2 cells (cluster 2), macrophages (cluster 1) and monocytes (cluster 3) (Figures 5E and 5F). Smyd3 ASO treatment did not significantly affect the cell abundance of each of these clusters (Figure S4D and Table S2). Of note, while macrophages demonstrated only a ~40% downregulation of *Smyd3* mRNA levels with Smyd3 ASO treatment (Table S1), differential gene expression within macrophages were still observed, suggesting that the observed changes in gene expression may be due to a more indirect effect of the Smyd3 ASO treatment, such as changes to other cell types or through changes in the tumor microenvironment.

To evaluate the effect of Smyd3 ASO treatment on the mononuclear myeloid cells of MOC1 tumors, we conducted differential gene expression analysis of selected immune-related genes comparing Smyd3 versus control ASO treated cells. No significant expression changes were observed in antigen-presentation machinery genes (Table S5). However, the evaluation of the expression changes in gene markers defining the M1 and M2 phenotypes showed that Smyd3 ASO treatment upregulated the expression of *Mrc1* (*Cd206*), *Arg1*, and *Cd163*, which characterize M2 macrophages (Figure 5G and Table S5). Additionally, *Gatm*, a gene encoding for glycine amidinotransferase which is a rate-limiting enzyme for creatinine synthesis that has been reported to promote M2 polarization,[26] was among the top 5 genes

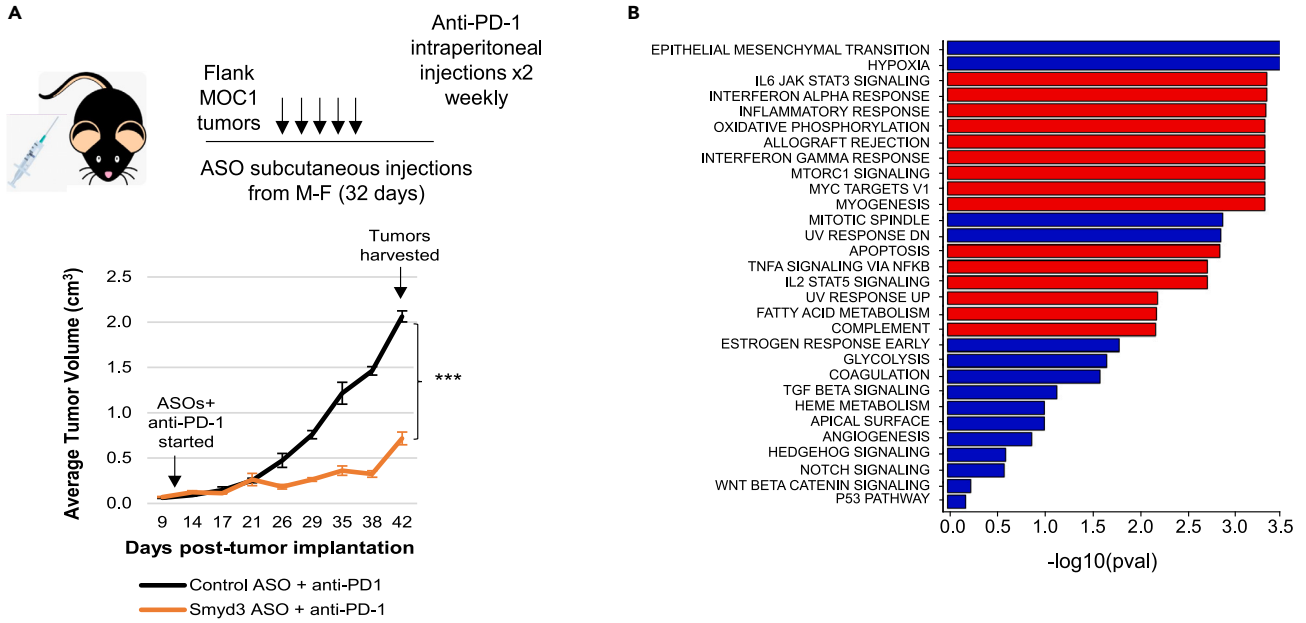
A
Anti-PD-1
intraperitoneal
injections x2
weekly
Flank
MOC1
tumors
ASO subcutaneous injections
from M-F (32 days)
Tumors
harvested
Average Tumor Volume (cm³)
2.5
2.0
1.5
1.0
0.5
0.0
***
ASOs+
anti-PD-1
started
9 14 17 21 26 29 35 38 42
Days post-tumor implantation
Control ASO + anti-PD1
Smyd3 ASO + anti-PD-1
B
EPITHELIAL MESENCHYMAL TRANSITION
HYPOXIA
IL6 JAK STAT3 SIGNALING
INTERFERON ALPHA RESPONSE
INFLAMMATORY RESPONSE
OXIDATIVE PHOSPHORYLATION
ALLOGRAFT REJECTION
INTERFERON GAMMA RESPONSE
MTORC1 SIGNALING
MYC TARGETS V1
MYOGENESIS
MITOTIC SPINDLE
UV RESPONSE DN
APOPTOSIS
TNFA SIGNALING VIA NFKB
IL2 STAT5 SIGNALING
UV RESPONSE UP
FATTY ACID METABOLISM
COMPLEMENT
ESTROGEN RESPONSE EARLY
GLYCOLYSIS
COAGULATION
TGF BETA SIGNALING
HEME METABOLISM
APICAL SURFACE
ANGIOGENESIS
HEDGEHOG SIGNALING
NOTCH SIGNALING
WNT BETA CATENIN SIGNALING
P53 PATHWAY
0.0 0.5 1.0 1.5 2.0 2.5 3.0 3.5
-log10(pval)
C
HALLMARK_INTERFERON_ALPHA_RESPONSE
H: hallmark gene sets, SMYD3-CONTROL, ES=0.87, NES=3.57, pval=0.00047, padj 0.009
Enrichment Score (ES)
Rank
Gene score
zero crossed at 6638
N=73
HALLMARK_INTERFERON_GAMMA_RESPONSE
H: hallmark gene sets, SMYD3-CONTROL, ES=0.83, NES=3.75, pval=0.00049, padj 0.009
zero crossed at 6638
N=130
Control ASOs + anti-PD-1
Smyd3 ASOs + anti-PD-1
D
Chemokines/Cytokines and Receptors
Exhaustion checkpoint and Receptors
T-cell activation checkpoints and Receptors
Control ASOs +
anti-PD-1
Smyd3 ASOs +
anti-PD-1

Figure 6. Combined Smyd3 ASO and anti-PD-1 treatment induces an inflammatory tumor microenvironment in MOC1 tumors

(A) Design of mouse experiment. Flank MOC1 tumors were established in C57BL/6 mice, and control or Smyd3 ASO treatment combined with anti-PD-1 was started with subcutaneous and intraperitoneal injections respectively. MOC1 tumors were captured after 32 days of treatment (day 42 post-implantation). Graph shows the average tumor size of 3 tumors per condition that underwent bulk RNA-seq. Student's t test, ***$p = 0.0002$.

(B) GSEA of MOC1 tumors treated with control or Smyd3 ASOs and anti-PD-1 reveals enrichment with inflammation-related Hallmark pathways. The x axis represents –log10 (*p*-values). Red bars indicate positive enrichment; blue bars indicate negative enrichment.

(C) Interferon α and γ response Hallmark pathways are upregulated in MOC1 tumors treated with Smyd3 ASOs and anti-PD-1 compared to control ASOs and anti-PD-1.

(D) Heatmaps of chemokines/cytokines, exhaustion, and T cell activation checkpoints and their respective receptors in MOC1 tumors treated with Smyd3 ($n = 3$) or control ASOs ($n = 3$) and anti-PD-1.

significantly upregulated in cluster 1 macrophages. Also, *Ccl24*, the most significantly upregulated gene, was recently reported to promote an M2 phenotype through the interaction of macrophages with eosinophils, the main producers of this chemokine[27] (Figure 5G and Table S5). These changes suggest that the Smyd3 ASO treatment of MOC1 tumors may favor the polarization of macrophages toward the M2 phenotype.

In summary, these results support that the Smyd3 ASO treatment of MOC1 tumors induces transcriptomic changes supporting an IFN-responsive state of cancer cells, as well as an activated anti-tumor state of $CD8^+$ T-cells and a shift toward an anti-tumor neutrophil phenotype within the MOC1 tumor microenvironment. However, $CD4^+$ T cell and macrophage differentiation seem to be shifted toward pro-tumorigenic phenotypes (Treg and M2 differentiation), suggesting these as possible mechanisms of resistance to Smyd3 depletion therapies.

Smyd3 ASO treatment induces the upregulation of *Cxcl9* and *Cxcl10* predominantly in cancer cells

We previously showed that SMYD3 depletion induced the upregulation of *CXCL9* and *CXCL10* in human HPV-negative HNSCC cell lines.[10,28] Given the importance of CXCL9 and CXCL10 in inducing $CD8^+$ T cell influx and converting "cold" to "hot" tumors,[29] we assessed whether the respective genes were also upregulated in cells obtained from Smyd3 ASO treated MOC1 tumors. Interestingly, *Cxcl9* was predominantly expressed in endothelial cells, macrophages, and cancer cells (Figure S6; Table S6). As expected, Smyd3 ASO treatment induced the upregulation of *Cxcl9*, but this was observed predominantly in cancer cells, with a statistically significant increase by nearly 1.6-fold (Wilcoxon test, $p < 0.001$, Table S6). *Cxcl10* was predominantly expressed in endothelial cells, neutrophils, and cancer cells (Figure S6; Table S6). Similar to *Cxcl9*, the greatest upregulation of *Cxcl10* expression was observed in cancer cells nearly 2-fold (Wilcoxon test, $p < 0.001$, Table S6). While neutrophils also showed a nearly 1.4-fold upregulation of *Cxcl10*, this did not reach statistical significance (Figure S6; Table S6). Interestingly, other cell types, including macrophages and $CD8^+$ T-cells, which are considered to be the cell types with the greatest contribution of these chemokines in the tumor microenvironment,[29] did not show significant upregulation of *Cxcl9* and *Cxcl10* after Smyd3 ASO treatment. Notably, cancer cells were among the cell types with more than 50% *Smyd3* mRNA downregulation after Smyd3 ASO treatment, in contrast to macrophages which manifested less than 50% downregulation of *Smyd3* mRNA. However, $CD8^+$ T-cells also manifested more than 50% decrease in *Smyd3* mRNA levels. This suggests a cell-type specific effect of Smyd3 ASOs on cancer cells with regards to the modulation of gene expression of *Cxcl9* and *Cxcl10*.

Combined Smyd3 ASO and anti-PD-1 treatment induce the upregulation of multiple chemokines, cytokines, and immune checkpoints in a syngeneic mouse model of flank HPV-negative MOC1 tumors

The above results support that Smyd3 ASO monotherapy induces the upregulation of type I IFN response genes, including *Cxcl9* and *Cxcl10*, in MOC1 cancer cells, which can explain the influx of $CD8^+$ T-cells in MOC1 tumors. Smyd3 ASOs also upregulate APM genes in MOC1 cancer cells, which may enhance antigen presentation by cancer cells, and reinvigorate $CD8^+$ T-cells toward a more cytotoxic phenotype. These results provide mechanistic insights into how Smyd3 ASO monotherapy sensitizes MOC1 tumors to anti-PD-1 therapy. To elucidate the global changes in the TME of flank MOC1 tumors induced by the addition of anti-PD-1 to Smyd3 ASOs, we conducted bulk RNA-seq of MOC1 tumors treated with control or Smyd3 ASOs and anti-PD-1 for approximately 4 weeks (32 days of treatment) (Figure 6A and S7A–S7D). As expected for an anti-PD-1 resistant tumor model, the growth curve of PBS treated tumors was similar to those of PBS + anti-PD-1 and control ASO + anti-PD-1 (Figure S7A). GSEA showed the enrichment of inflammatory Hallmark pathways, such as the IL6-JAK-STAT3 signaling and the type I and type II IFN response pathways (Figures 6B and 6C) in MOC1 tumors treated with the combination of Smyd3 ASOs and anti-PD-1. Interestingly, hypoxia and glycolysis pathways, which adversely affect antitumor immune responses, were also downregulated in the Smyd3 ASO and anti-PD-1 treated MOC1 tumors (Figure 6B).

Accordingly, differential gene expression analysis of immune-related gene panels revealed the upregulation of genes coding for multiple chemokines, cytokines, and their respective receptors, such as *Cxcl9, Cxcl10, Cxcl11, Cxcr3,* and *Ccl5* (Figure 6D). Importantly, the genes coding for *Ifn-β(Il6), Ifn-γ*, and its receptor Ifngr1, which are primary activators of inflammation within the tumor microenvironment, were also upregulated. Furthermore, MOC1 tumors treated with Smyd3 ASOs and anti-PD-1 showed the upregulation of genes coding for multiple immune checkpoints and their receptors, including *Pdcd1, Cd274, Pdcd1lg2, Havcr2 (Tim3), Lgals9* (*galectin-9*), *Tigit, Lag3, Ido1*, and *Cd86 (B7-H2)*. Genes coding for T cell activation checkpoints, such as *Tnfsf4, Cd27, Cd28, Cd40, Cd48*, and *Icos*, were also found upregulated in MOC1 tumors treated with Smyd3 ASOs and anti-PD-1 compared with tumors treated with control ASOs and anti-PD-1 (Figure 6D).

To evaluate whether these expression changes were associated with the expansion of specific T cell receptor (TCR) clones, TCR-receptor sequencing of MOC1 tumors treated with control ($n = 8$) or Smyd3 ASOs ($n = 6$) and anti-PD-1 was conducted. Results revealed a trend toward

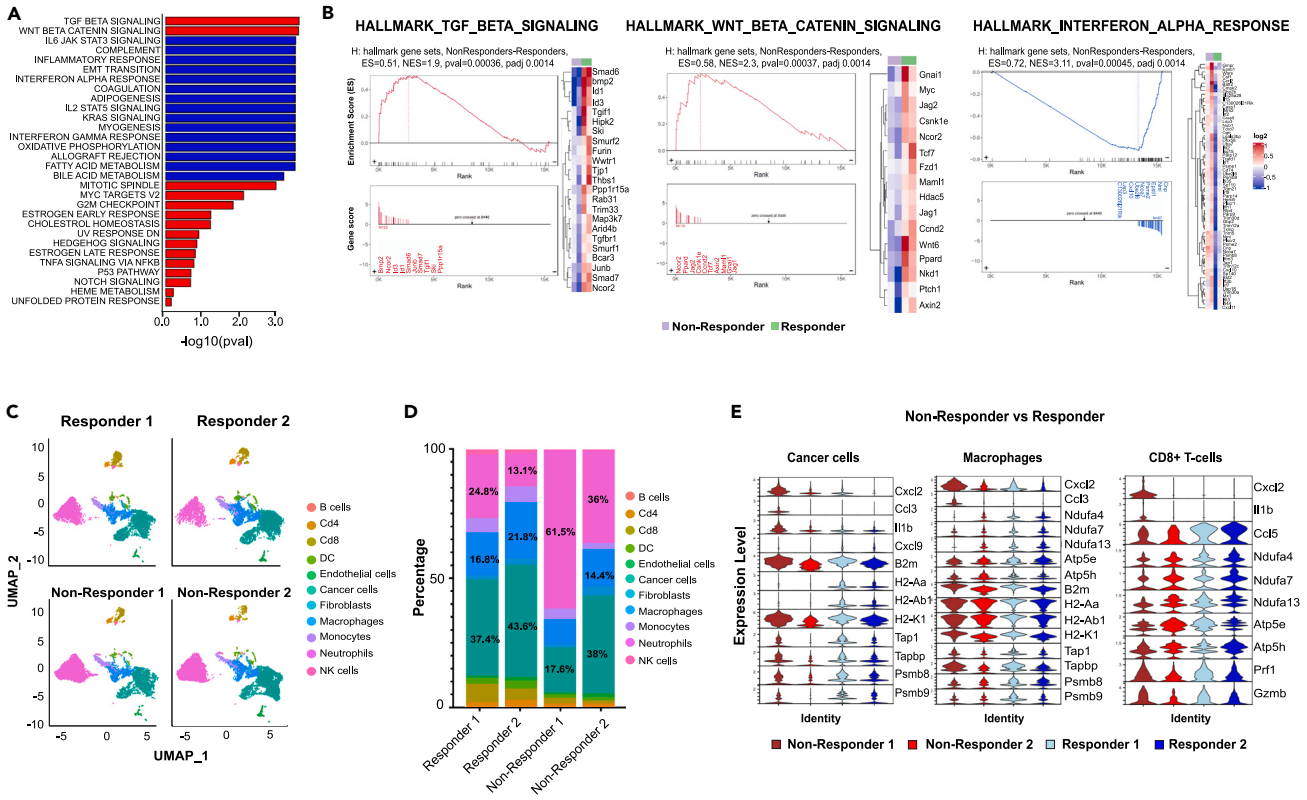

Figure 7. Non-responder MOC1 tumors exhibit variable mechanisms of resistance to Smyd3 ASOs and anti-PD-1

(A) GSEA using Hallmark gene sets is shown. The x axis represents –log10 (*p*-values). The red bars indicate pathways positively enriched in non-responder MOC1 tumors, while the blue bars indicate pathways negatively enriched in non-responder MOC1 tumors compared to responder MOC1 tumors ($n = 2$).

(B) Hallmark pathways and associated heatmaps enriched in non-responders compared to responder MOC1 tumors treated with Smyd3 ASOs and anti-PD-1.

(C) UMAP of MOC1 non-responders (1 and 2) and responders (1 and 2) to Smyd3 ASOs and anti-PD-1 treatment.

(D) Percentage of cell types in responder and non-responder MOC1 tumors.

(E) Violin plots showing genes among the top 30 that were found differentially expressed in non-responder compared to responder MOC1 tumors.

increased clonality of TCR clones in the Smyd3 ASO + anti-PD-1 treated MOC1 tumors, however, this did not reach statistical significance (Wilcoxon test, $p = 0.059$) (Figure S8).

Overall, these data support that the treatment of flank MOC1 tumors with the systemic administration of Smyd3 ASOs and anti-PD-1 in this syngeneic MOC1 mouse model of HPV-negative HNSCC induces the intratumoral upregulation of multiple genes encoding for $CD8^+$ T cell attracting chemokines, immune and T cell activation checkpoints, as well as *Ifn-β* and *Ifn-γ*, when compared to MOC1 tumors treated with control ASOs and anti-PD-1 alone.

MOC1 tumors resistant to Smyd3 ASOs and anti-PD-1 are enriched in the WNT-β catenin and TGF-β pathways

Based on our recent report, while 75% of MOC1 tumors treated with the combination treatment of Smyd3 ASOs and anti-PD-1 showed significant tumor shrinkage or complete regression, 25% of tumors were resistant to the treatment (non-responder tumors).[10] To dissect pathways associated with the non-responder versus responder state of MOC1 tumors, we analyzed the bulk RNA-seq data from two responder and two non-responder MOC1 tumors to the combined treatment with Smyd3 ASOs and anti-PD-1 (32 days of treatment, Figures S7A–S7D). GSEA revealed that non-responder tumors were positively enriched in the TGF-β and the WNT-β catenin Hallmark pathways, which are associated with immune escape.[30–32] Additionally, multiple immune-related pathways, such as the IL6-JAK-STAT3 signaling pathway and the IFN-α and IFN-γ response pathways, were repressed (Figures 7A and 7B).

Single-cell RNA sequencing of non-responder MOC1 tumors reveals variable mechanisms of resistance derived from different cell types

To further dissect the contribution of different cell types in the resistance of MOC1 tumors to Smyd3 ASOs and anti-PD-1 combined treatment, we conducted single-cell RNA-seq analysis of two responders (termed 1 and 2) and two non-responder (termed 1 and 2) MOC1 tumors treated with Smyd3 ASOs and anti-PD-1, obtained from an independent *in vivo* experiment with mice treated for 29 days (Figure S9). UMAP

analysis of these MOC1 tumors identified the same cell types previously identified in MOC1 tumors treated with ASOs (Figure 7C). Regarding the abundance of different cell types, non-responder tumors had numerically fewer $CD8^+$ T-cells, $CD4^+$ T-cells, dendritic, and NK cells compared to responder tumors. One of the non-responder tumors (tumor 1) had substantially more neutrophils compared to the responder MOC1 tumors (Figure 7D and Table S7).

To assess the transcriptomic differences in the MOC1 cancer cell populations of non-responder and responder MOC1 tumors treated with Smyd3 ASOs and anti-PD-1, we conducted differential gene expression and GSEA analysis comparing each of the two non-responder tumors to both responder tumors (Figures 7E, S10, S11, and Table S8). Results revealed multiple possible mechanisms of resistance. For non-responder tumor 1, cancer cells were enriched in Gene Ontology Biological Process pathways related to inflammatory response and neutrophil chemotaxis and migration (Figures S10 and S11). Consistently, neutrophil chemoattractants *Cxcl2*, *Ccl3,* and *Il1b* were amongst the top significantly upregulated genes in MOC1 cancer cells, consistent with the increased number of neutrophils in this non-responder tumor (Figure 7E and Table S8). Consistent with the lower $CD8^+$ T cell counts of this tumor, $CD8^+$ T cell attracting chemokine genes *Cxcl9*, *Cxcl10,* and *Ccl5* were amongst the most significantly repressed genes (Figure 7E and Table S8). Similar to the MOC1 cancer cells, $CD8^+$ T-cells of the non-responder tumor 1 were characterized by pathways related to neutrophil chemotaxis, with the upregulation of *Cxcl2* and *Il1b*, and significant repression of *Ccl5*, a major $CD8^+$ T cell chemoattractant chemokine (Figures 7E, S10, and Table S8). Interestingly, genes encoding for a number of NADH dehydrogenase subunits, such as *Ndufa4*, *Ndufa7* and *Ndufa13*, as well as genes encoding for subunits of ATP synthase, such as *Atp5e* and *Atp5h*, were significantly repressed (Figure 7E and Table S8). Consistently, $CD8^+$ T-cells of non-responder tumor 1 also demonstrated repression of Gene Ontology Biologic Process pathways related to aerobic respiration and oxidative phosphorylation, suggesting a switch to anaerobic metabolism (Figure S10). Macrophages in this non-responder tumor were also characterized by the upregulation of neutrophil chemoattractants *Cxcl2* and *Ccl3*, and by repression of genes encoding for subunits of NADH dehydrogenase, and the ATP synthase, such as *Ndufa4*, *Ndufa7*, *Ndufa13*, *Atp5e* and *Atp5h*, and resultant negative enrichment of the oxidative phosphorylation and the ATP biosynthetic process, suggesting the presence of a tumor microenvironmental factor affecting the metabolic behavior of $CD8^+$ T-cells and macrophages (Figures 7E, S10, and Table S8). Importantly, *Mrc1* and *Arg1* were upregulated, supporting a macrophage shift toward the M2 pro-tumor phenotype (Table S8). Neutrophils were positively enriched in Gene Ontology Biologic Process pathways related to migration and proliferation; however, a pathway signifying active innate immune response was repressed, suggesting decreased functionality of these neutrophils (Figure S10; Table S8).

MOC1 cancer cells and macrophages of non-responder tumor 2 were characterized by repression of antigen presentation machinery pathways, with *B2m*, *MHC class I* genes, *Tap1*, *Tapbp*, *Psmb8,* and *Psmb9* being among the most significantly repressed genes. IFN-β and IFN-γ immune response pathways were also repressed in both cancer cells and macrophages (Figures 7E, S11, and Table S8). Expectedly, $CD8^+$ T-cells of non-responder 2 were characterized by significant repression of *Prf1*, *Gzmb,* and *Ccl5* (Table S7). Neutrophils of non-responder tumor 2 were characterized by the negative enrichment of pathways related to IFN-β/IFN-γ and innate immune response (Figure S11; Table S8).

Overall, these findings support that individual cell types of MOC1 tumors implement versatile mechanisms to escape the therapeutic efficacy of Smyd3 ASOs and anti-PD-1 combined treatment, which may include the attraction of pro-tumorigenic neutrophils, aberrant metabolism, and the repression of antigen presentation. In non-responder tumor 1, neutrophil chemoattractant coding genes *Cxcl2*, *Ccl3*, and *Il1b* were found consistently upregulated in cancer cells, macrophages, and $CD8^+$ T-cells. Further gene expression analysis showed that these neutrophils demonstrated the upregulation of *Ccl3* and *Tnf*, consistent with a pro-tumorigenic N2 phenotype (Table S8). Cancer cells and $CD8^+$ T-cells were also characterized by significant repression of genes encoding for $CD8^+$ T cell attracting chemokines *Cxcl9, Cxcl10,* and *Ccl5*. $CD8^+$ T-cells and macrophages demonstrated repression of genes encoding for subunits of NADH dehydrogenase and the ATP synthase, such as *Ndufa4*, *Ndufa7*, *Ndufa13*, *Atp5e,* and *Atp5h*. Macrophages in this non-responder tumor 1 demonstrated the upregulation of markers consistent with M2 differentiation, as also observed in MOC1 tumors treated with Smyd3 ASO monotherapy. In non-responder tumor 2, cancer cells and macrophages demonstrated repression of antigen presentation machinery genes as a predominant mechanism of resistance. Finally, although the upregulation of *Ctla4* was observed in MOC1 tumors treated with Smyd3 ASO monotherapy, the possible role of Tregs as contributors of resistance to the combination Smyd3 ASO and anti-PD-1 therapy could not be further surmised, as *Ctla4* and *Foxp3* mRNA expression levels were not detectable in the scRNA-seq databases of non-responder tumors.

DISCUSSION

While pembrolizumab has established a new treatment paradigm for HPV-negative HNSCC, only 20% of patients with recurrent/metastatic disease respond, and an even smaller fraction achieve durable responses. There is thus an urgent need for novel interventions to enhance therapeutic efficacy. SMYD3 is a protein lysine methyltransferase that is overexpressed in multiple cancer types, including HPV-negative HNSCC and has been shown to render poor survival.[10,13–19,33] While a number of reports have explored the oncogenic functions of SMYD3, very few studies have examined its immunomodulatory functions in cancer.[10] Our group recently reported that SMYD3 depletion derepresses type I IFN response and APM genes in HPV-negative HNSCC cancer cells *in vitro* and that Smyd3 ASOs induce an influx of $CD8^+$ T-cells and sensitize MOC1 tumors to anti-PD-1 therapy.[10,34] In this study, we further dissected the effect of Smyd3 ASOs alone and in combination with anti-PD-1 in the tumor microenvironment of MOC1 tumors, evaluated the differential effects of Smyd3 ASOs in different cell types, and identified potential mechanisms of resistance.

We have found that MOC1 tumors treated with Smyd3 ASOs and anti-PD-1 are enriched in IFN-alpha and IFN-gamma response gene signatures, and upregulate genes encoding for key immune-related cytokines, chemokines, and checkpoints, such as *Ifn-β*, *Ifn-γ*, *Cxcl9, Cxcl10*, and *Ccl5*, suggesting the generation of an inflamed tumor microenvironment. Smyd3 ASOs had a variable effect on the degree of

Smyd3 mRNA downregulation by cell type, with T-cells, neutrophils, and cancer cells manifesting the greatest degree of downregulation, suggesting differential uptake of the Smyd3 ASOs by each cell type. On the cancer cell compartment, Smyd3 ASO treatment induced enrichment in type I IFN response gene signatures and upregulation of multiple type I IFN response and APM genes, consistent with our previously reported work.[10] MOC1 tumors generated from *Smyd3* KO MOC1 cell lines were significantly sensitized to anti-PD-1 treatment, suggesting that the Smyd3 ASO-induced changes in the MOC1 cancer cells are sufficient to sensitize MOC1 tumors to anti-PD-1 treatment. Importantly, this antitumor effect was $CD8^+$ T cell but not $CD4^+$ T cell dependent.

In regard to the immune-cell compartment, Smyd3 ASO treatment induced gene expression changes consistent with a shift of exhausted $CD8^+$ T-cells toward a more activated and cytotoxic state with a greater survival capacity. The central memory/progenitor $CD8^+$ T cell cluster showed expression changes consistent with an activated/memory phenotype with increased proliferative capacity. Furthermore, neutrophils acquired gene signatures indicative of neutrophil activation, while the expression of gene markers of N2 differentiation was decreased. These findings suggest that Smyd3 promotes a pro-tumor phenotype in $CD8^+$ T-cells and neutrophils. On the other hand, the $CD4^+$ T cell compartment acquired gene expression changes indicative of a shift toward a more tolerant, Treg phenotype. Smyd3 ASO monotherapy also seemed to induce gene expression changes promoting an M2 pro-tumorigenic macrophage phenotype. These findings support that Smyd3 ASOs may potentiate an antitumor immune response mediated by $CD8^+$ T-cells and activated neutrophils; however, they may also inadvertently promote immune escape through Treg and M2 macrophage differentiation. This finding may explain the lack of significant anti-tumor efficacy observed on flank MOC1 tumors in the syngeneic mouse model treated with Smyd3 ASOs (Figure 1A).

We then evaluated potential mechanisms of resistance of MOC1 tumors treated with Smyd3 ASOs in combination with anti-PD-1 by comparing non-responder to responder tumors. We found that individual cell types of MOC1 tumors implement versatile mechanisms to escape the therapeutic efficacy of Smyd3 ASOs and anti-PD-1 combined treatment, including the upregulation of genes coding for neutrophil chemoattractants and the promotion of a protumorigenic neutrophil phenotype, and the repression of genes coding for $CD8^+$ T cell chemoattractants, subunits of NADH dehydrogenase and the ATP synthase, and antigen presentation machinery components. Additionally, a shift toward M2 macrophage differentiation was also observed, similar to our findings in MOC1 tumors treated with Smyd3 ASO monotherapy. Furthermore, the TGF-β and Wnt signaling pathways were found positively enriched in MOC1 tumors that escaped the therapeutic treatment effect of Smyd3 ASOs and anti-PD-1. Although the upregulation of *Ctla4* was observed in MOC1 tumors treated with Smyd3 ASO monotherapy, the possible role of Tregs as contributors of resistance to the combination Smyd3 ASO and anti-PD-1 therapy could not be further surmised, as *Ctla4* and *Foxp3* mRNA expression levels were not detectable in the scRNA-seq databases of non-responder tumors. Combinatorial approaches tailored toward these mechanisms of resistance, such as targeting protumorigenic neutrophils, M2 macrophages, and the TGF-β and Wnt signaling pathways may further increase the therapeutic efficacy of Smyd3 depletion and anti-PD-1 combination strategies.

In summary, Smyd3 depletion using ASOs induces an IFN-responsive state in cancer cells, it may reinvigorate exhausted $CD8^+$ T-cells toward a more cytotoxic phenotype and promote an anti-tumor neutrophil phenotype *in vivo*. On the other hand, Smyd3 ASO monotherapy may concurrently promote a Treg and M2 macrophage phenotype. These findings underscore the paradigm of how certain treatments promote both anti-tumorigenic as well as pro-tumorigenic effects, the latter possibly constituting causes of treatment resistance. Furthermore, we identify potential mechanisms of resistance to the Smyd3 ASO and anti-PD-1 combination treatment of MOC1 tumors, which include the attraction of pro-tumorigenic neutrophils, aberrant metabolism, the repression of $CD8^+$ T cell attracting chemokines and of antigen presentation, M2 macrophage polarization and the upregulation of TGF-β and Wnt signaling pathways. Interestingly, our study supports that certain mechanisms of resistance may be derived from different cell types within the tumor microenvironment. Conversely, other resistance mechanisms may be shared by certain cell types within the tumor microenvironment, such as the upregulation of genes coding for neutrophil chemoattractants or the repression of genes coding for $CD8^+$ T cell attracting chemokines observed in both cancer cells and $CD8^+$ T-cells. These mechanisms provide insight into combinatorial approaches that could increase the therapeutic efficacy of the Smyd3 ASO and anti-PD-1 combination treatment. With Smyd3 ASOs representing a promising drug platform,[10,11,20] this work constitutes an additional stepping stone toward the translation of SMYD3 ASOs to clinical trials for patients with HPV-negative HNSCC in combination with anti-PD-1 therapies.

Limitations of the study

A number of limitations would need to be acknowledged in this study. First, the phenotypic changes surmised in the T cell, macrophage, and neutrophil compartments with Smyd3 ASO treatment, such as the differentiation toward activated/memory $CD8^+$ T-cells, the anti-tumorigenic phenotype of neutrophils, and the induction of Tregs and M2 macrophages, were based on transcriptomic analysis and have not been validated at the protein level. Further validation to ascertain these phenotypic shifts and to evaluate the role of the immune cell compartment in the antitumor efficacy of the Smyd3 ASO and anti-PD-1 combination would require flow cytometry and mouse experiments that allow for the conditional depletion of Smyd3 in each of the individual immune cell types, as well as the depletion of Smyd3 using ASOs in the syngeneic mouse model of *Smyd3* KO MOC1 tumors treated with anti-PD-1. Additionally, given the protagonistic role of $CD8^+$ T-cells in the antitumor efficacy of anti-PD-1 therapy, it would be necessary to functionally assess the effect of Smyd3 ASOs and anti-PD-1 combination therapy on the cytotoxic function of $CD8^+$ T-cells against cancer cells, compared to Smyd3 ASOs or anti-PD-1 alone, using *ex vivo* cytotoxicity assays. Furthermore, the variability in the uptake of the Smyd3 ASOs by different cell types introduces an additional level of complexity in discerning which effects are directly versus indirectly induced by the Smyd3 ASOs and would require spatial proteomics approaches to further dissect how the dynamic cell-cell interactions within the TME are affected by Smyd3 depletion. Second, the specific mechanism(s) through which Smyd3 depletion induces the described transcriptomic changes within each cell type of the TME would need to be further investigated.

Given our previously published report,[10] Smyd3 functions as an epigenetic regulator of immune-related gene expression in cancer cells. Genome-wide mapping of Smyd3 would be necessary to support its possible epigenetic function in immune cells too. Third, while we describe a number of plausible escape mechanisms to the Smyd3 ASO and anti-PD-1 combination therapy, our findings were based on only two, highly variable non-responder MOC1 tumors; analysis of more non-responder MOC1 tumors would be required to further validate these findings. The translational applicability of these observations would also need to be further explored and validated in human HPV-negative HNSCC tumors. Fourth, the question of whether the observed changes in the tumor microenvironment are dependent or independent of the enzymatic activity of Smyd3 has not been addressed, and is necessary to pursue using SMYD3 enzymatic inhibitors. Also, mouse experiments would be necessary to assess whether Smyd3 ASO + anti-PD-1 treatment prolongs the survival of treated mice, induces antitumor memory by rechallenging cured mice, whether the discontinuation of the combination therapy is associated with sustained antitumor efficacy, and evaluate whether the anti-PD-1 therapy alone can induce antitumor efficacy in a previously responsive mouse that has been inoculated with a second MOC1 tumor. Finally, these findings require further validation in additional syngeneic HPV-negative HNSCC mouse models, as well as in mouse models of other squamous cell carcinomas with similar genetic backgrounds as HPV-negative HNSCC, such as lung and bladder squamous cell carcinomas.

RESOURCE AVAILABILITY

Lead contact

Further information and requests for resources and reagents should be directed and will be fulfilled by the Lead Contact, Vassiliki Saloura (vassiliki.saloura@nih.gov).

Materials availability

CRISPR KO cell lines generated in this study are available from the lead contact with a completed Materials Transfer Agreement.

Data and code availability

- Bulk, single-cell RNA-seq have been deposited at GEO with accession ID# GSE273232, GSE273507, and GSE273508 and will be publicly available as of the date of publication.
- This article does not report the original code.
- All raw data reported in this article will be shared by the lead contact upon request. Any additional information required to reanalyze the data reported in this article is available from the lead contact upon request.

ACKNOWLEDGMENTS

This work was funded by the Intramural Research Program of the National Cancer Institute. This work was also supported by the NCI Center for Cancer Research (CCR) and has been funded in whole or in part with Federal funds from the National Cancer Institute at the National Institutes of Health, under Contract No. 75N91019D00024. The content of this publication does not necessarily reflect the views or policies of the Department of Health and Human Services, nor does mention of trade names, commercial products, or organizations imply endorsement by the U.S. Government.

AUTHOR CONTRIBUTIONS

DT: Data curation, investigation, formal analysis, methodology, validation, visualization, and writing-original draft, AL: data analysis, methodology, and visualization, AA: data analysis, methodology, and visualization, JA: data analysis and visualization, MSD: data analysis and investigation, ML: visualization, KM: investigation, formal analysis, methodology, and visualization, SK: data analysis and visualization, YR: investigation, AH: investigation, BB: investigation, AS: data analysis, methodology, and visualization, MM: investigation, BK: investigation and formal analysis, XL: investigation and methodology, CA: investigation and methodology, VS: data curation, investigation, formal analysis, methodology, validation, visualization, and writing-original draft.

DECLARATION OF INTERESTS

Xiaolin Luo was an employee of Ionis Pharmaceuticals Inc during this study. The other authors declare no competing interests.

STAR★METHODS

Detailed methods are provided in the online version of this paper and include the following:

- KEY RESOURCES TABLE
- EXPERIMENTAL MODEL AND STUDY PARTICIPANT DETAILS
  - Generation of *Smyd3* knockout cell lines using CRISPR
  - Cell lines
  - *In vivo* mouse experiments
- METHOD DETAILS
  - Single-cell RNA sequencing
  - Bulk RNA sequencing
  - TCR sequencing
  - Western blotting
  - Validation of Smyd3 ASO knockdown efficacy at the protein level
  - Interferon-β treatment
  - Multicolor flow cytometry
- QUANTIFICATION AND STATISTICAL ANALYSIS
  - List of type I IFN response and APM genes

- RNA-seq analysis
- Gene Set Enrichment Analysis
- Single-cell RNA-sequencing analysis
- TCR-sequencing analysis
- Statistical analyses for *in vitro* and *in vivo* experiments

SUPPLEMENTAL INFORMATION

Supplemental information can be found online at https://doi.org/10.1016/j.isci.2024.110854.

Received: June 13, 2024
Revised: July 4, 2024
Accepted: August 28, 2024
Published: August 30, 2024

REFERENCES

1. Siegel, R.L., Miller, K.D., and Jemal, A. (2018). Cancer statistics, 2018. CA A Cancer J. Clin. *68*, 7–30. https://doi.org/10.3322/caac.21442.
2. Ang, K.K., and Sturgis, E.M. (2012). Human papillomavirus as a marker of the natural history and response to therapy of head and neck squamous cell carcinoma. Semin. Radiat. Oncol. *22*, 128–142. https://doi.org/10.1016/j.semradonc.2011.12.004.
3. Burtness, B., Harrington, K.J., Greil, R., Soulières, D., Tahara, M., de Castro, G., Jr., Psyrri, A., Basté, N., Neupane, P., Bratland, Å., et al. (2019). Pembrolizumab alone or with chemotherapy versus cetuximab with chemotherapy for recurrent or metastatic squamous cell carcinoma of the head and neck (KEYNOTE-048): a randomised, open-label, phase 3 study. Lancet *394*, 1915–1928. https://doi.org/10.1016/s0140-6736(19)32591-7.
4. Cao, J., and Yan, Q. (2020). Cancer Epigenetics, Tumor Immunity, and Immunotherapy. Trends Cancer *6*, 580–592. https://doi.org/10.1016/j.trecan.2020.02.003.
5. Peng, D., Kryczek, I., Nagarsheth, N., Zhao, L., Wei, S., Wang, W., Sun, Y., Zhao, E., Vatan, L., Szeliga, W., et al. (2015). Epigenetic silencing of TH1-type chemokines shapes tumour immunity and immunotherapy. Nature *527*, 249–253. https://doi.org/10.1038/nature15520.
6. Nagarsheth, N., Peng, D., Kryczek, I., Wu, K., Li, W., Zhao, E., Zhao, L., Wei, S., Frankel, T., Vatan, L., et al. (2016). PRC2 Epigenetically Silences Th1-Type Chemokines to Suppress Effector T-Cell Trafficking in Colon Cancer. Cancer Res. *76*, 275–282. https://doi.org/10.1158/0008-5472.Can-15-1938.
7. Chiappinelli, K.B., Strissel, P.L., Desrichard, A., Li, H., Henke, C., Akman, B., Hein, A., Rote, N.S., Cope, L.M., Snyder, A., et al. (2015). Inhibiting DNA Methylation Causes an Interferon Response in Cancer via dsRNA Including Endogenous Retroviruses. Cell *162*, 974–986. https://doi.org/10.1016/j.cell.2015.07.011.
8. Topper, M.J., Vaz, M., Chiappinelli, K.B., DeStefano Shields, C.E., Niknafs, N., Yen, R.W.C., Wenzel, A., Hicks, J., Ballew, M., Stone, M., et al. (2017). Epigenetic Therapy Ties MYC Depletion to Reversing Immune Evasion and Treating Lung Cancer. Cell *171*, 1284–1300.e21. https://doi.org/10.1016/j.cell.2017.10.022.
9. Griffin, G.K., Wu, J., Iracheta-Vellve, A., Patti, J.C., Hsu, J., Davis, T., Dele-Oni, D., Du, P.P., Halawi, A.G., Ishizuka, J.J., et al. (2021). Epigenetic silencing by SETDB1 suppresses tumour intrinsic immunogenicity. Nature *595*, 309–314. https://doi.org/10.1038/s41586-021-03520-4.
10. Nigam, N., Bernard, B., Sevilla, S., Kim, S., Dar, M.S., Tsai, D., Robbins, Y., Burkitt, K., Sievers, C., Allen, C.T., et al. (2023). SMYD3 represses tumor-intrinsic interferon response in HPV-negative squamous cell carcinoma of the head and neck. Cell Rep. *42*, 112823. https://doi.org/10.1016/j.celrep.2023.112823.
11. Crooke, S.T., Witztum, J.L., Bennett, C.F., and Baker, B.F. (2018). RNA-Targeted Therapeutics. Cell Metabol. *27*, 714–739. https://doi.org/10.1016/j.cmet.2018.03.004.
12. Sun, L., Clavijo, P.E., Robbins, Y., Patel, P., Friedman, J., Greene, S., Das, R., Silvin, C., Van Waes, C., Horn, L.A., et al. (2019). Inhibiting myeloid-derived suppressor cell trafficking enhances T cell immunotherapy. JCI Insight *4*, e126853. https://doi.org/10.1172/jci.insight.126853.
13. Sarris, M.E., Moulos, P., Haroniti, A., Giakountis, A., and Talianidis, I. (2016). Smyd3 Is a Transcriptional Potentiator of Multiple Cancer-Promoting Genes and Required for Liver and Colon Cancer Development. Cancer Cell *29*, 354–366. https://doi.org/10.1016/j.ccell.2016.01.013.
14. Bernard, B.J., Nigam, N., Burkitt, K., and Saloura, V. (2021). SMYD3: a regulator of epigenetic and signaling pathways in cancer. Clin. Epigenet. *13*, 45. https://doi.org/10.1186/s13148-021-01021-9.
15. Mazur, P.K., Reynoird, N., Khatri, P., Jansen, P.W.T.C., Wilkinson, A.W., Liu, S., Barbash, O., Van Aller, G.S., Huddleston, M., Dhanak, D., et al. (2014). SMYD3 links lysine methylation of MAP3K2 to Ras-driven cancer. Nature *510*, 283–287. https://doi.org/10.1038/nature13320.
16. Hamamoto, R., Furukawa, Y., Morita, M., Iimura, Y., Silva, F.P., Li, M., Yagyu, R., and Nakamura, Y. (2004). SMYD3 encodes a histone methyltransferase involved in the proliferation of cancer cells. Nat. Cell Biol. *6*, 731–740. https://doi.org/10.1038/ncb1151.
17. Wang, Y., Xie, B.H., Lin, W.H., Huang, Y.H., Ni, J.Y., Hu, J., Cui, W., Zhou, J., Shen, L., Xu, L.F., et al. (2019). Amplification of SMYD3 promotes tumorigenicity and intrahepatic metastasis of hepatocellular carcinoma via upregulation of CDK2 and MMP2. Oncogene *38*, 4948–4961. https://doi.org/10.1038/s41388-019-0766-x.
18. Foreman, K.W., Brown, M., Park, F., Emtage, S., Harriss, J., Das, C., Zhu, L., Crew, A., Arnold, L., Shaaban, S., and Tucker, P. (2011). Structural and functional profiling of the human histone methyltransferase SMYD3. PLoS One *6*, e22290. https://doi.org/10.1371/journal.pone.0022290.
19. Jiang, Y., Lyu, T., Che, X., Jia, N., Li, Q., and Feng, W. (2019). Overexpression of SMYD3 in Ovarian Cancer is Associated with Ovarian Cancer Proliferation and Apoptosis via Methylating H3K4 and H4K20. J. Cancer *10*, 4072–4084. https://doi.org/10.7150/jca.29861.
20. Kontaki, H., Koukaki, M., Vasilarou, M., Giakountis, A., Deligianni, E., Luo, X., Kim, Y., and Talianidis, I. (2021). Targeting Smyd3 by next-generation antisense oligonucleotides suppresses liver tumor growth. iScience *24*, 102473. https://doi.org/10.1016/j.isci.2021.102473.
21. Keck, M.K., Zuo, Z., Khattri, A., Stricker, T.P., Brown, C.D., Imanguli, M., Rieke, D., Endhardt, K., Fang, P., Brägelmann, J., et al. (2015). Integrative analysis of head and neck cancer identifies two biologically distinct HPV and three non-HPV subtypes. Clin. Cancer Res. *21*, 870–881. https://doi.org/10.1158/1078-0432.Ccr-14-2481.
22. Chung, C.H., Parker, J.S., Karaca, G., Wu, J., Funkhouser, W.K., Moore, D., Butterfoss, D., Xiang, D., Zanation, A., Yin, X., et al. (2004). Molecular classification of head and neck squamous cell carcinomas using patterns of gene expression. Cancer Cell *5*, 489–500. https://doi.org/10.1016/s1535-6108(04)00112-6.
23. Shaul, M.E., Levy, L., Sun, J., Mishalian, I., Singhal, S., Kapoor, V., Horng, W., Fridlender, G., Albelda, S.M., and Fridlender, Z.G. (2016). Tumor-associated neutrophils display a distinct N1 profile following TGFβ modulation: A transcriptomics analysis of pro- vs. antitumor TANs. OncoImmunology *5*, e1232221. https://doi.org/10.1080/2162402x.2016.1232221.
24. Masucci, M.T., Minopoli, M., and Carriero, M.V. (2019). Tumor Associated Neutrophils. Their Role in Tumorigenesis, Metastasis, Prognosis and Therapy. Front. Oncol. *9*, 1146. https://doi.org/10.3389/fonc.2019.01146.
25. Zilionis, R., Engblom, C., Pfirschke, C., Savova, V., Zemmour, D., Saatcioglu, H.D., Krishnan, I., Maroni, G., Meyerovitz, C.V., Kerwin, C.M., et al. (2019). Single-Cell Transcriptomics of Human and Mouse Lung Cancers Reveals Conserved Myeloid Populations across Individuals and Species. Immunity *50*, 1317–1334.e10. https://doi.org/10.1016/j.immuni.2019.03.009.

26. Yu, L., Wang, L., Hu, G., Ren, L., Qiu, C., Li, S., Zhou, X., Chen, S., and Chen, R. (2022). Reprogramming alternative macrophage polarization by GATM-mediated endogenous creatine synthesis: A potential target for HDM-induced asthma treatment. Front. Immunol. *13*, 937331. https://doi.org/10.3389/fimmu.2022.937331.
27. Lee, S.H., Chaves, M.M., Kamenyeva, O., Gazzinelli-Guimaraes, P.H., Kang, B., Pessenda, G., Passelli, K., Tacchini-Cottier, F., Kabat, J., Jacobsen, E.A., et al. (2020). M2-like, dermal macrophages are maintained via IL-4/CCL24-mediated cooperative interaction with eosinophils in cutaneous leishmaniasis. Sci. Immunol. *5*, eaaz4415. https://doi.org/10.1126/sciimmunol.aaz4415.
28. Vougiouklakis, T., Bao, R., Nakamura, Y., and Saloura, V. (2017). Protein methyltransferases and demethylases dictate CD8+ T-cell exclusion in squamous cell carcinoma of the head and neck. Oncotarget *8*, 112797–112808. https://doi.org/10.18632/oncotarget.22627.
29. Reschke, R., and Gajewski, T.F. (2022). CXCL9 and CXCL10 bring the heat to tumors. Sci. Immunol. *7*, eabq6509. https://doi.org/10.1126/sciimmunol.abq6509.
30. Batlle, E., and Massagué, J. (2019). Transforming Growth Factor-β Signaling in Immunity and Cancer. Immunity *50*, 924–940. https://doi.org/10.1016/j.immuni.2019.03.024.
31. Spranger, S., Bao, R., and Gajewski, T.F. (2015). Melanoma-intrinsic β-catenin signalling prevents anti-tumour immunity. Nature *523*, 231–235. https://doi.org/10.1038/nature14404.
32. Luke, J.J., Bao, R., Sweis, R.F., Spranger, S., and Gajewski, T.F. (2019). WNT/β-catenin Pathway Activation Correlates with Immune Exclusion across Human Cancers. Clin. Cancer Res. *25*, 3074–3083. https://doi.org/10.1158/1078-0432.Ccr-18-1942.
33. Fenizia, C., Bottino, C., Corbetta, S., Fittipaldi, R., Floris, P., Gaudenzi, G., Carra, S., Cotelli, F., Vitale, G., and Caretti, G. (2019). SMYD3 promotes the epithelial-mesenchymal transition in breast cancer. Nucleic Acids Res. *47*, 1278–1293. https://doi.org/10.1093/nar/gky1221.
34. Nagata, D.E.d.A., Ting, H.A., Cavassani, K.A., Schaller, M.A., Mukherjee, S., Ptaschinski, C., Kunkel, S.L., and Lukacs, N.W. (2015). Epigenetic control of Foxp3 by SMYD3 H3K4 histone methyltransferase controls iTreg development and regulates pathogenic T-cell responses during pulmonary viral infection. Mucosal Immunol. *8*, 1131–1143. https://doi.org/10.1038/mi.2015.4.
35. Judd, N.P., Allen, C.T., Winkler, A.E., and Uppaluri, R. (2012). Comparative analysis of tumor-infiltrating lymphocytes in a syngeneic mouse model of oral cancer. Otolaryngol. Head Neck Surg. *147*, 493–500. https://doi.org/10.1177/0194599812442037.

STAR★METHODS

KEY RESOURCES TABLE

REAGENT or RESOURCE	SOURCE	IDENTIFIER
Antibodies		
InVivoMAb Plus anti-mouse PD-1	Bio X Cell	Cat# BE0146; RRID:AB_10949053
InVivoMAb Plus anti-CD8α	Bio X Cell	Cat# BE0117; RRID:AB_10950145
InVivoMAb Plus anti-CD4	Bio X Cell	Cat# BE0003-3; RRID:AB_1107642
anti-H3K4me1	Abcam	Cat# ab8895; RRID:AB_306847
ECL Anti-Rabbit IgG, Horseradish Peroxidase linked F(ab')$_2$	Cytiva	Cat# NA9340V
Mouse anti-Smyd3	Abcam	Cat# ab187149; RRID:AB_3083695
Alexa 488 anti-PDL1	BD	Cat# 566864; RRID:AB_2869917
PE-Dazzle 594 anti-PD1	BioLegend	Cat# 135228; RRID:AB_2566006
PE-Cy5 anti-PDGFR (CD140a)	BioLegend	Cat#135920; RRID:AB_2814033
APC anti-CD11b	BioLegend	Cat# 101212; RRID:AB_312795
Alexa 700 anti-CD3e	BioLegend	Cat# 152316; RRID:AB_2632713
APC-Cy7 anti-CD25	BioLegend	Cat# 102026; RRID:AB_830745
BV510 anti-F4/80	BioLegend	Cat# 123135; RRID:AB_2562622
BV605 anti-CD11c	BioLegend	Cat# 117334; RRID:AB_2562415
BV750 anti-CD31	BD	Cat# 746871; RRID:AB_2871671
BV786 anti-CD45.2	BioLegend	Cat# 109839; RRID:AB_2562604
LIVE/DEAD Fixable Blue Dead Cell Stain Kit	Invitrogen	Cat# L23105
BUV661 anti-CD8a	BD	Cat# 750023; RRID:AB_2874241
BUV737 anti-H2-Kb (MHC I)	BD	Cat# 748822; RRID:AB_2873225
BUV805 anti-CD4	BD	Cat# 612900; RRID:AB_2827960
Deposited data		
Bulk RNA-seq data of MOC1		Deposited under accession ID# GSE273232
Sc-RNA-seq data of MOC1		Deposited under accession ID# GSE273507
Sc-RNA-seq data of 2 responder and 2 non-responder tumors		Deposited under accession ID#GSE273508
Experimental models: cell lines		
MOC1 cell line	Dr. Clint T. Allen, NIDCD	CVCL_ZD32
Experimental models: organisms/strains		
C57BL/6 mice	Taconic	
Oligonucleotides		
Control ASOs	Ionis Pharmaceuticals	
Smyd3 ASOs	Ionis Pharmaceuticals	
Recombinant DNA		
SMYD3 KO CRISPR Plasmid	Nigam et al. 2023[10]	https://doi.org/10.1016/j.celrep.2023.112823
Software and algorithms		
ImageJ	NIH	https://imagej.nih.gov/ij/
FACSDiva	BD biosciences	https://www.bdbiosciences.com/en-us/products/software/instrument-software/bd-facsdiva-software#Overview

(*Continued on next page*)

Continued

REAGENT or RESOURCE	SOURCE	IDENTIFIER
FlowJo V.X10.0.7r2	BD biosciences	https://www.flowjo.com/solutions/flowjo/downloads/previous-versions
Other		
Fetal bovine serum	Cytiva	SH30071.03
Penicillin/streptomycin	Vita Scientific	120-095-721
L-glutamine	Thermo Fisher Scientific	17605E
Lipofectamine RNAimax	Thermo Fisher Scientific	13778150
Trypsin EDTA 0.25%	Sigma	T8003
Nuclear complex Co-IP kit	Active Motif	54001
Direct-zol RNA miniprep kit	Zymo Research	R2072
Matrigel Extracellular Matrix	Corning	354277
Mouse tumor dissociation kit	Miltenyi Biotec	130-096-730
IMDM Medium	Gibco	12440-053
Ham's F-12 nutrient mix	Cytiva	SH30026.02
Hydrocortisone	Sigma-Aldrich	H0888
Exponential growth factor	Sigma-Aldrich	E9644-5MG
Insulin solution from bovine panceas	Sigma-Aldrich	I0516-5ML
Recombinant mouse interferon-β	R&D systems Inc.	8234-MB/CF
gentleMACS Dissociator	Miltenyi Biotec	
RPMI-1640	Gibco	11875-093
Gentamycin	Gibco	15710-064
Hepes buffer	Corning	25-060-CI
MEM nonessential amino acids	Corning	25-025-CI
Sodium pyruvate	Corning	25-000-CI
2-Mercaptoethanol	Sigma-Aldrich	M6250-10ML

EXPERIMENTAL MODEL AND STUDY PARTICIPANT DETAILS

Generation of *Smyd3* knockout cell lines using CRISPR

Smyd3 CRISPR knockout cell lines (*Smyd3* KO 10, 13) were generated from parental MOC1 cells using clustered regularly interspaced short palindromic repeats (CRISPR/Cas9) technology. Transfected MOC1 cells were subjected to single-cell selection of GFP expressing cells using flow cytometry. GFP-positive cells were grown from a single-cell in culture. SMYD3 expression levels of individual clones were measured by Western blotting to confirm efficacy of knockout (Figure S12). A control cell line (NC2) was concurrently generated with a non-targeting sgRNA.

Cell lines

MOC1 is a transplantable mouse HPV-negative squamous cell carcinoma cell line derived from carcinogen-induced primary tumors in C57BL/6 WT mice.[35] MOC1, NC2, KO10 and KO13 cell lines were maintained in a solution of 62% IMDM medium, 31% Ham's F-12 nutrient mix, 5% fetal bovine serum, 1% penicillin/streptomycin, 40 μg/L hydrocortisone, 5 μg/L exponential growth factor (EGF), and 5 mg/L insulin.

In vivo mouse experiments

All mouse experiments and procedures performed were conducted in a fully accredited animal housing facility at the National Institutes of Health, Bethesda, MD. All animal experimental protocols were approved by the NCI-Bethesda Animal Care and Use Committee. 4-6 week-old female C57BL/6 mice were purchased from Taconic and used for the described experiments. The study designs and animal usage were conducted accordingly to all applicable guidelines by the NCI-Bethesda Animal Care and Use Committee. Mice were randomly assigned to experimental groups. An established, DMBA (7,12-dimethylbenz(a)anthracene)-induced, mouse oral carcinoma 1 (MOC1) cell line in a syngeneic C57BL/6 mouse model of MOC1 flank tumors was utilized.[35] MOC1 cells were grown *in vitro* and were inoculated by subcutaneous injections of 5 million MOC1 cells in suspension using Matrigel Extracellular Matrix (cat#356234, Corning, Durham, NC) in the right flanks of C57BL/6 mice. Once flank tumors reached an average volume of 0.1cm^3, mice were randomized into treatment groups and treatment was initiated according to each experiment. Mice were treated with control ASOs or Smyd3 ASOs at a concentration of 12.5 m/kg for 5 days

per week with subcutaneous injections, as previously described.[10] Intraperitoneal injections of anti-PD-1 (InVivoPlus anti-mouse PD-1, RMP1-14, BioXCell) were conducted at 200ug/injection, twice weekly. Tumor length (L) and width (W) were measured twice weekly with calipers and tumor volumes were calculated using the formula LxW^2/2. Weights were measured twice weekly.

For the *Smyd3* KO MOC1 tumor experiments, we utilized two *Smyd3* KO clones (KO10 and KO13) and a control MOC1 clone generated using non-targeting sgRNAs (NC2). KO10, KO13 and NC2 cells were grown *in vitro* and were inoculated by subcutaneous injections of 5 million cells in suspension using Matrigel (Corning) in the right flanks of C57BL/6 mice. Once flank tumors reached an average volume of 0.1cm^3, mice were randomized into treatment groups and treatment was initiated with anti-PD-1 as described above. Mice were randomized to the following treatment groups: *Smyd3* KO 10 experiment: NC2 (n = 7), NC2 + anti-PD-1 (n = 8), KO10 (n = 5), KO10 + anti-PD-1. *Smyd3* KO13 experiment: NC2 (n = 8), NC2 + anti-PD-1 (n = 9), KO13 (N = 9), KO13 + anti-PD-1 (n = 9).

For the CD4$^+$ and CD8$^+$ T cell depletion experiment, the KO10 *Smyd3* KO cell line was used to generate flank tumors. When the average volume of flank tumors of all mice in the experiment reached 0.1 cm^3, mice were randomized into three groups and treatments were initiated. Intraperitoneal injections of anti-PD-1 (InVivoMAb Plus anti-mouse PD-1, BE0146, BioXCell, Lebanon, NH), anti-CD8α (InVivoMAb Plus anti-mouse CD8α, BE0117, BioXCell, Lebanon, NH), or anti-CD4 (InVivoMAb Plus anti-mouse CD4, BE0003-3, BioXCell, Lebanon, NH) were conducted at 200 μg/mouse, twice weekly. Mouse body weight was measured twice weekly with a digital scale. Tumor length (L), tumor width (W) were measured twice weekly with digital calipers. Tumor volume was calculated using the formula LxW^2/2.

METHOD DETAILS

Single-cell RNA sequencing

MOC1 tumors treated with control or Smyd3 ASOs (n = 3 per condition), or responder (n = 2) and non-responder MOC1 tumors (n = 2) treated with Smyd3 ASOs and anti-PD-1 were mechanically and chemically digested into single-cell suspensions using the gentleMACS Dissociator and the mouse tumor dissociation kit by Miltenyi Biotec (130-096-730, Miltenyi Biotec, Auburn, CA) respectively, per manufacturer's protocol. The samples' concentrations and viability were assessed using the LunaFL fluorescent cell counter. Cells were diluted 2 times and loaded in the 10X chip lanes according to the 10X Chromium 3′ v3.1 gene expression User Guide with one capture lane per sample. Partitioning was completed successfully with uniform emulsion consistency. Reverse transcription and barcoding were performed immediately. All subsequent steps of library preparation and quality control were performed as described in the 10X User Guide (3′ v3.1). Two NextSeq runs were performed.

Bulk RNA sequencing

Bulk RNA sequencing was performed on MOC1 tumors treated with control (n = 3) or Smyd3 ASOs (n = 5) and anti-PD-1. C57BL/6 mice with flank MOC1 tumors received subcutaneous injections of 12.5 mg/kg control or Smyd3 ASO, 5 days weekly, along with intraperitoneal injections of 200 mg/mouse anti-PD-1 (InVivoMAb Plus anti-mouse PD-1, BE0146, BioXCell, Lebanon, NH), twice weekly. On day 33 of treatment, mice were euthanized and flank MOC1 tumors were surgically resected and frozen in liquid nitrogen. Tumors were processed for RNA extraction. Specifically, approximately 30 mg of tissue was sub-sampled from tumor and placed into prechilled Lysing Matrix A tubes (MP Biomedical, cat# 116910050). Tissue was lysed in 1 mL of TRIzol Reagent (ThermoFisher, cat# 15596026) using a Bead Ruptor 12 (Omni) at high speed for 2 x 30 s. The aquaeous phase was separated by adding 200 mL of chloroform and centrifuging at 12,000 xg for 15 min at 4°C. RNA was extracted using the RNeasy Mini Kit (Qiagen, Cat# 74104) following the manufacturer's instructions with the addition of 1.5 mL volumes of 100% ethanol to the aqueous phase. RNA quantity and purity were determined by a NanoDrop spectrophotometer. RNA quality was analyzed by Agilent 6000 Pico Chip. RNA was stored at −80°C until subsequent assay/analyses. For bulk RNA sequencing, samples were pooled and sequenced on NextSeq 2000 P2 using TruSeq Stranded mRNA Prep and paired-end sequencing. The samples had 49 to 66 million pass filter reads with more than 94% of bases above the quality score of Q30. Reads of the samples were trimmed for adapters and low-quality bases using Cutadapt before alignment with the reference genome (mm10) and the annotated transcripts using STAR. The average mapping rate of all samples was 95%. Unique alignment was above 85%. There were 3.59–5.70% unmapped reads. The mapping statistics were calculated using Picard software. The samples had between 0.07 and 0.11% ribosomal bases. Percent coding bases were between 51 and 56%. Percent UTR bases are 33–39%, and mRNA bases were between 87 and 91% for all the samples. Library complexity was measured in terms of unique fragments in the mapped reads using Picard's MarkDuplicate utility. The samples had 67-73% non-duplicate reads. In addition, the gene expression quantification analysis was performed for all samples using STAR/RSEM tools.

TCR sequencing

TCR sequencing was performed on MOC1 tumors treated with control (n = 8) or Smyd3 ASOs (n = 6) and anti-PD-1. C57BL/6 mice with flank MOC1 tumors received subcutaneous injections of 12.5 mg/kg control or Smyd3 ASO, 5 days weekly, along with intraperitoneal injections of 200 mg/mouse anti-PD-1 (InVivoMAb Plus anti-mouse PD-1, BE0146, BioXCell, Lebanon, NH), twice weekly. On day 33 of treatment, mice were euthanized and flank MOC1 tumors were surgically resected and frozen in liquid nitrogen. Tumors were processed for DNA extraction. Specifically, approximately 30 mg of tissue was added to 1 mL of 0.2 mg/mL Proteinase K (Qiagen) in TD-S0 (Autogen). Sample tubes were placed into a Thermomixer R (Eppendorf, North America). The tissue was digested at 56°C overnight, with 5min of shaking at 850 rpm every 30min. DNA was isolated using the phenol-based AutoGenprep 245T Animal Tissue DNA Extraction Kit (Autogen) according to the manufacturer's instructions. DNA was suspended in 200 mL of 10 mM Tris, pH 8.0. Yield and purity were determined by NanoDrop One

spectrophotometer (ThermoFisher). DNA was stored at −20°C until subsequent assay/analyses. TCR sequencing was conducted using Adaptive Immuunosequencing per manufacturer's protocol.

Western blotting

Nuclear extracts were prepared using the Nuclear Complex Co-IP kit (54001, Active Motif, Carlsbad, CA) and 10 μg of each extract was loaded to examine protein levels of Smyd3. Primary antibodies used were anti-Smyd3 (ab187149, Abcam, Cambridge, MA, dilution 1:1000) and anit-histone H3 (ab8895, Abcam, Cambridge, MA, dilution 1:50000). Horseradish Peroxidase linked $F(ab')_2$ fragment anti-rabbit IgG (NA9340V, Cytiva, Malborough, MA, dilution 1:5000) was used as a secondary antibody. Densitometry was performed using ImageJ software (NIH, Bethesda, MD).

Validation of Smyd3 ASO knockdown efficacy at the protein level

MOC1 cells were plated in 10cm dishes and treated with PBS, 0.5uM, 1uM or 2uM of control or Smyd3 ASOs. After 3 days of treatment, cells were collected and nuclear extracts were obtained as described above. Western blotting for Smyd3 as described above was conducted with 10ug of nuclear extract, using H3 as a loading control (Figure S13A). Immunohistochemistry for Smyd3 was also conducted in a MOC1 tumor treated with control + anti-PD-1 (#855) versus Smyd3 ASOs + anti-PD-1 (#987) (S 8). For the Smyd3 immunohistochemistry (Figure S13B), the staining was performed on Leica Bond RX automated stainer. After deparaffinization and rehydration, tissue sections were treated with antigen retrieval solution (Leica Microsystems) with heat near 100°C for 20 min. The anti-SMYD3 antibody (1:400) was applied on tissue sections for 1 h incubation at room temperature. The antigen-antibody binding was detected with Leica Bond Polymer Refine Detection system (Leica Microsystems) and the slides were covered with cover glasses. Stained slides were digitized using the Aperio AT2 whole slide scanner (Leica Biosystems). Subsequently, image analysis was conducted using the CytoNuclear algorithm (version 2.0.9) within the Halo imaging analysis software (Indica Labs, Albuquerque, NM). The algorithm was configured to identify weak, moderate, and strong positive cells. The final data captured the percentage of strong positive cells. Additionally, a pathologist (B.K) performed image annotations, excluding fields with artifacts such as folds or tears.

Interferon-β treatment

Recombinant mouse interferon-β (8234-MB/CF, R&D systems Inc., Minneapolis, MN) was added to NC2, KO10 and KO13 cells in 10 cm dishes at a concentration of 1000U/mL for 24 h prior to collection for Western blotting.

Multicolor flow cytometry

For the multicolor flow of MOC1 tumors, mice were euthanized and flank MOC1 tumors were surgically resected, and mechanically and chemically digested into single-cell suspensions using the gentleMACS Dissociator and the mouse tumor dissociation kit (Miltenyi Biotec), per manufacturer's protocol. Single-cell suspensions were filtered through 70um filters and washed with 1% BSA in PBS. Samples were incubated with anti-CD16/32 (Biolegend) antibody to block nonspecific staining. Subsequently, the primary antibodies were added and incubation for 30min was carried out in the dark. Cell surface staining was performed using fluorophore-conjugated Alexa 488 anti-mouse PDL1 (BD 566864), PE-Dazzle 594 PD1 (BioLegend 135228), PE-Cy5 PDGFR/CD140a (BioLegend 135920), PE-Cy7 I-Ab/MHC II (BioLegend 116420), APC CD11b (BioLegend 101212), Alexa 700 CD3e (BioLegend 152316), APC-Cy7 CD25 (BioLegend 102026), BV510 F4/80 (BioLegend 123135), BV605 CD11c (BioLegend117334), BV750 CD31 (BD 746871), BV786 CD45.2 (BioLegend 109839), BUV661 CD8a (BD 750023), BUV737 H2-Kb/MHC I (BD 748822), and BUV805 CD4 (BD 612900). Cell viability was assessed with LIVE/DEAD Fixable Blue Dead Cell Stain Kit (L23105, Invitrogen, Waltham, MA). All analyses was performed on a BD Fortessa analyzer (BD Biosceinces, Franklin Lakes, NJ) running FACSDiva software and interpreted using FlowJo V.X10.0.7r2.

QUANTIFICATION AND STATISTICAL ANALYSIS

List of type I IFN response and APM genes

To generate dotplots, we interrogated the gene set from the HALLMARK INTERFERON ALPHA RESPONSE (IFNα response genes) and the KEGG ANTIGEN PROCESSING AND PRESENTATION (APM genes), which are available in the Molecular Signature Database (MSigDB) gene sets (Table S4, https://www.gsea-msigdb.org/gsea/msigdb/index.jsp). Genes that were not found to be expressed at the mRNA level in the RNA-seq databases of each cell system presented in these figures were omitted.

RNA-seq analysis

RNA-Seq data were quantitated to obtain raw tag counts at the gene level using featureCounts (v2.0.2). The voom transformation (limma R package v3.38.3) that incorporates precision weights based on the observed mean-variance relationship in the data was applied to the original count data. Additionally, the counts were normalized using the quantile normalization method, and a heatmap for top 500 most variable genes was created using a pheatmap R package v1.0.12 with Euclidean distance and ward.D2 clustering options.

Gene Set Enrichment Analysis

Gene set enrichment analysis (GSEA) was performed using "fgsea" R library on genes identified with "run_de" procedure from "Libra" R package. Default settings were used. HALLMARK and the Gene Ontology Biological Processes (GOBP) gene lists were obtained from the Broad Institute website (mSigDB collection, https://data.broadinstitute.org/gsea-msigdb/). X axes values represent normalized enrichment scores (NES) or -log10(*p*-value). Red color indicates positive and blue color indicates negative enrichment.

Single-cell RNA-sequencing analysis

Base calling was performed using RTA 3.9.25, demultiplexing was done using cellranger v7.0.0 (Bcl2fastq 2.20.0), and alignment was performed using cellranger v7.0.0 (STAR 2.7.2a). Sequenced reads were aligned to the 10x Genomics provided mouse reference sequence (refdata-gex-mm10-2020-A). Expression data were analyzed using the Seurat package (version 4.1.3) according to the package manual, including dimensionality reduction, clustering, and cell type identification steps. The raw sequencing data, generated from individual cells, underwent initial quality control and preprocessing steps to filter out low-quality cells and normalize gene expression values. Clustering of cells was performed to identify distinct cell populations based on their gene expression profiles. Differential gene expression analysis was conducted to unravel molecular signatures characterizing each identified cluster. Cell Types were annotated using SingleR (ver. 2.4.1) according to the package manual. ImmGen_Main set was selected for annotation.

TCR-sequencing analysis

A down-sampling tool in ImmunoSeq Analyzer (ANALYSES 3.0) was used to obtain unique productive rearrangements of down-sampled data.

Statistical analyses for *in vitro* and *in vivo* experiments

The Wilcoxon test was used to compare cell types treated with Smyd3 or control ASOs to evaluate *Smyd3* mRNA expression changes. The Student's t test was used to compare differences in the cell numbers of clusters treated with Smyd3 or control ASOs. The unpaired t-test was used to compare tumor volumes, and immune and cancer cell markers of MOC1 tumors treated with control ASOs or Smyd3 ASOs.